Nucleic Acids Research, 2024, **52**, 7031–7048
https://doi.org/10.1093/nar/gkae474
Advance access publication date: 3 June 2024
Genome integrity, repair and replication

The translocation activity of Rad54 reduces crossover outcomes during homologous recombination

Krishay Sridalla†, Mitchell V. Woodhouse†, Jingyi Hu, Jessica Scheer, Bryan Ferlez and J.Brooks Crickard*

Deparment of Molecular Biology and Genetics, Cornell University, Ithaca, NY 14853, USA

*To whom correspondence should be addressed. Tel: +1 607 254 4679; Email: jbc287@cornell.edu
†The first two authors should be regarded as Joint First Authors.

Abstract

Homologous recombination (HR) is a template-based DNA double-strand break repair pathway that requires the selection of an appropriate DNA sequence to facilitate repair. Selection occurs during a homology search that must be executed rapidly and with high fidelity. Failure to efficiently perform the homology search can result in complex intermediates that generate genomic rearrangements, a hallmark of human cancers. Rad54 is an ATP dependent DNA motor protein that functions during the homology search by regulating the recombinase Rad51. How this regulation reduces genomic exchanges is currently unknown. To better understand how Rad54 can reduce these outcomes, we evaluated several amino acid mutations in Rad54 that were identified in the COSMIC database. COSMIC is a collection of amino acid mutations identified in human cancers. These substitutions led to reduced Rad54 function and the discovery of a conserved motif in Rad54. Through genetic, biochemical and single-molecule approaches, we show that disruption of this motif leads to failure in stabilizing early strand invasion intermediates, causing increased crossovers between homologous chromosomes. Our study also suggests that the translocation rate of Rad54 is a determinant in balancing genetic exchange. The latch domain's conservation implies an interaction likely fundamental to eukaryotic biology.

Graphical abstract

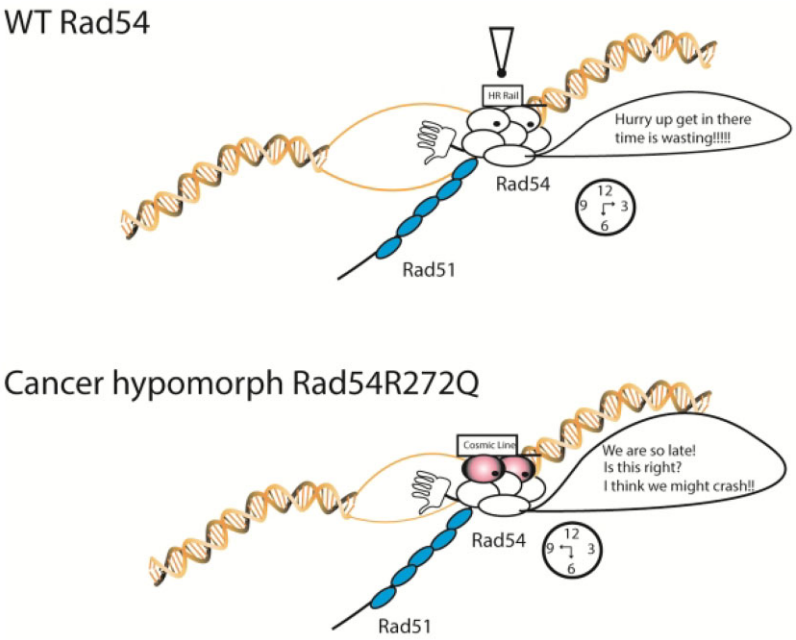

Introduction

Homologous recombination (HR) is a template-based DNA double strand break repair (DSBR) pathway based on locating a matching sequence element elsewhere in the genome (1–4). To find a DNA template, HR proceeds through a series of steps that begins with the identification of a double-strand break followed by a 5′ to 3′ resection of the DNA to create ssDNA overhangs (5,6). The ssDNA is then loaded with recombinase filaments, Rad51 in eukaryotes, which use the ssDNA as a guide to search the genome for a template to facilitate DNA repair (7–11). Once a template is found, Rad51, in conjunction with numerous accessory factors, promotes a

Received: January 29, 2024. **Revised:** May 16, 2024. **Editorial Decision:** May 17, 2024. **Accepted:** May 21, 2024

strand invasion reaction, which results in further base pairing between the recipient ssDNA and the donor dsDNA as well as displacement of the non-template strand, resulting in the formation of a structure known as the displacement loop (D-loop) (12–15).

Formation of the D-loop during HR is a dynamic process that requires the selection of an appropriate template and stabilization of strand pairing events in a process called the homology search (7–11,16–22). A successful homology search leads to the extension of D-loops, which allows the transition to the DNA repair and resolution phase of HR (23). In *Saccharomyces cerevisiae*, the steps in forming D-loops are regulated by many DNA translocases and helicases, including Rad54 (24), Rdh54 (14,25–27), and Srs2 (13,28–32). These ATP-dependent motors control reaction intermediates, including Rad51 filaments (28,29,32,33) and D-loop structures (13,33,34). Each of these motors also impacts HR outcomes with the deletion of *RDH54*, resulting in increased break-induced replication (BIR), and deletion of *SRS2*, resulting in increased DNA crossovers (CO) between donor and recipient DNA molecules (35). Importantly, increases in these outcomes can have mutagenic consequences on the genome. The role of Rad54 in preventing these outcomes is poorly defined, given its general importance to D-loop formation, extension, and disruption. Thus, making it difficult to disentangle early steps from late steps.

Rad54 is a Snf2 family DNA motor protein that functions as a multimeric motor during the HR to promote DNA and chromatin remodeling (36–39), Rad51 remodeling (40–42), and D-loop stabilization (15,34,40,43). It should be noted that there is still open debate about how Rad54 is involved in the homology search and whether it contributes to both DNA sequence alignment and D-loop stabilization or just D-loop stabilization *in vivo* (11,34,44). Deletion of Rad54 creates a reduction in D-loop formation, leading to failure in HR mediated repair (34) and causing chromosome loss (45). Genetic evidence suggests that overexpression of the catalytically inactive Rad54K341R increases crossovers between homologous chromosomes (46), a type of genetic exchange. A dominant negative effect could cause this as Rad54 functions as a multimer (8,47,48), and overexpression of a catalytically inactive protein would poison WT proteins by reducing the rate of ATP hydrolysis and translocation (8). This has been interpreted as a disruption in the synthesis-dependent strand annealing pathway (SDSA), generally accepted to produce non-crossover outcomes during DNA repair (1,2,7,49). However, this could also result from increased non-crossover resolution as part of the classical double strand break repair pathway (DSBR) (50). This observation is consistent with the requirement for Rad54 activity to prevent complex genetic exchanges (46). The mechanism by which Rad54 prevents excessive strand exchange is currently unclear. However, Rad54 is known to promote branch migration, and it is speculated that this activity may promote non-crossover outcomes due to a reduction in the extent of DNA exchange between donor and recipient DNA (47,51,52).

The multiple roles of Rad54 during HR have led to the development of the idea that this motor acts as a general catalyst to speed up the DNA repair reaction. This is consistent with the model that Rad54 works as a sister chromatid exchange factor (53,54). To better define the role of Rad54 in mitigating genetic exchange, we sought to identify and characterize amino acid substitutions in Rad54 from human cancers that slowed down the translocation activity of Rad54. Our data suggests that reducing the Rad54 translocation activity leads to a kinetic delay in strand invasion, which can result in genetic exchanges characterized as crossovers between homologous chromosomes. We develop a model from which factors that stabilize early strand invasion intermediates may kinetically prevent complex rearrangements within the genome.

Materials and methods

Yeast strain construction

All recombination outcome experiments were performed in the W303 background. Strains for spot assay experiments were BY4741 and were generated by transforming *rad54*Δ strains with pRS415 plasmids. For integrated spot assays, *rad54* mutations were introduced by gene replacement into BY4741 strains. The genotypes for all strains used in this study can be found in Supplementary Table S1. Plasmids for the generation of strains can be found in Supplementary Table S2.

Yeast spot growth assay and colony growth

For complementation spot assays, overnight cultures were diluted back to an OD_{600} of 0.2 and then allowed to grow to an OD_{600} of 1.0. Cells were then serially diluted and manually spotted on YNB (–Leu) + 2% dextrose plates containing no drug, 0.003% or 0.01% methylmethanesulfonate (MMS). Plates were incubated at 30°C for 2–3 days and imaged at 24, 48 and 72 h. The same protocol was followed for integrated constructs, except the cells were grown and spotted on YPD plates. In the case of Rad51 overexpression experiments. pYes2-RAD51 plasmids were transformed into strains with *rad54R272Q* and *rad54R272A* alleles integrated into the genome. Spot assays were performed as described above, except cultures were spotted on YNB (–Ura) +/-2% dextrose or YNB (–Ura) ± 2% galactose. The plates were grown for 48 and 72 h and imaged. Human amino acid numbers can be found in Supplementary Table S3.

Red/white recombination assay

The WT strain used in this assay and the procedure for diploid formation are described here (27). The genotypes for modifying these strains can be found in Supplementary Table S2. The assay was performed by growing the appropriate strain overnight in YP + 2% raffinose. The next day, cells were diluted to an OD600 of 0.2 and allowed to reach an OD_{600} of 0.4–0.5, followed by the expression of *I-Sce1* by adding 2% galactose. Cells were allowed to grow for an additional 1.5 h, then plated on YPD plates, and allowed to grow for 48 h. After 48 h, they were placed at 4°C overnight to enable further development of the red color. The number of white, red, and sectored colonies was then counted followed by replica plating onto YPD + hygromycin B (200 μg/ml) and YPD + nourseothricin (67 μg/ml, clonNat) for analysis of recombination outcomes. Strains were also replica plated on YNB (–Ura/–Met) + 2% dextrose to ensure proper chromosome segregation (Supplementary Tables S4–S6). The data was analyzed by counting sectored colonies and colony survival on different antibiotic sensitivities. The data for each category was then divided by the total population of sectored colonies. The standard deviation between biological replicates was analyzed for at least three independent experiments from different crosses.

Protein purification

Rad51, Rad54 and RPA purifications were performed as previously described (8).

Electrophoresis mobility shift assay (EMSA) for Rad54

An Atto647N labeled 90-mer oligo was annealed with an unlabeled complementary oligo to make a labeled dsDNA substrate. The sequences of the oligos used in this assay can be found in Supplementary Table S7. The assay was performed in EMSA buffer (35 mM Tris–Cl [pH 7.5], 3 mM $MgCl_2$, 50 mM KCl, 1 mM DTT, 10% glycerol). The final DNA concentration was 10 nM and proteins were titrated to be 0, 6.25, 12.5, 25 and 50 nM as final concentrations. The DNA and proteins were incubated at 30°C for 5 min and then resolved by 10% Native-PAGE (20 mM Tris, 10 mM acetic acid, 0.5 mM EDTA, 10% acrylamide/bis-acrylamide (37.5:1), 0.1% APS, 0.1% TEMED) and ran in 0.5x TAE buffer (20 mM Tris, 10 mM acetic acid, 0.5 mM EDTA).

ATPase assay

A commercially available ADP-GLO kit was used to measure ATP hydrolysis rates. The ATP hydrolysis reaction was performed in HR buffer (20 mM Tris-OAc, 50 mM NaCl, 10 mM $MgOAc_2$, 200 ng/μl BSA, 1 mM DTT and 10% glycerol) and contained 1 mg/ml sheared salmon sperm DNA and 10 nM Rad54.

In vitro D-loop assay

D-loop formation experiments were performed in HR buffer (30 mM Tris-OAc [pH 7.5], 50 mM NaCl, 10 mM $MgOAc_2$, 1 mM DTT, 0.2 mg/ml BSA) using an Atto647N labeled DNA duplex (15 nM) with homology to the pUC19 plasmid. Rad51 (300 nM) was incubated with recipient DNA at 30°C for 15 min. The resulting Rad51 filaments were mixed with indicated concentrations of Rad54, RPA (500 nM), and pUC19 plasmid (0.3 nM). Reactions were quenched after indicated periods and treated with 1 unit of Proteinase K at 37°C for 20 min. The reactions were then resolved by electrophoresis on a 0.9% agarose gel and imaged for fluorescence using a Typhoon imager. The sequences of the oligos used in this study can be found in Supplementary Table S7.

Flow cell construction

Metallic chrome patterns were deposited on quartz microscope slides with pre-drilled holes for microfluidic line attachment by electron beam lithography to generate flow cells. After metal deposition, a channel was created by covering the two-sided tape with a small piece of paper between the drill holes. The paper was excised to make the flow chamber, and a glass coverslip was fixed to the tape. The chamber was sealed by heating to 165°C in a vacuum oven at 25 mmHg for 60 min. Flow cells were then completed using hot glue to fit IDEX nano ports over the drill holes on the opposite side of the microscope slide from the coverslip.

Single molecule experiments

All single molecule experiments were conducted on a custom-built prism-based total internal reflection microscope (Nikon) equipped with a 488-nm laser (Coherent Sapphire, 100 mW), a 561-nm laser (Coherent Sapphire, 100 mW), a 640-nm laser (Coherent Obis, 100 mW) and two Andor iXon EMCCD cameras. DNA substrates for DNA curtains experiments were made by attaching a biotinylated oligo to one end of the 50 kb Lambda phage genome and an oligo with a digoxygenin moiety on the other. This allowed double tethering of the DNA between chrome barriers and chrome pedestals, as previously described (55,56). Flow cells were attached to a microfluidic system, and sample delivery was controlled using a syringe pump (KD Scientific). Three-color imaging was achieved by two XION 512 × 512 back-thinned Andor EM-CCD cameras and alternative illumination using a 488-nm laser, a 561 nM laser, and a 640 nM laser at 25% power output. The lasers were shuttered, resulting in a 200 msec delay between each frame. Images were collected with a 200 msec integration time. Translocation velocity and distances were measured in HR Buffer (20 mM Tris-OAc [pH 7.5], 50 mM NaCl, 10 mM $MgOAc_2$, 200 ng/μl BSA, 1 mM DTT). Channel bleed through is prevented by shuttering of the laser lines, emission filters and the use of complementary fluorophores. In this case GFP is not activated by the 561 or 647 laser lines, and Atto647N is not activated by the 488 or 561 laser lines. mCherry labelled fluorophores can be poorly activated by the 488-laser line. However, the emitted light is split by a dichroic mirror and filtered through a band pass and long pass filter to block wavelengths of light above a certain cutoff. This is sufficient to prevent mCherry signal bleed through into the 488 channel.

Analysis of dsDNA translocation

The velocity and track length for GFP-Rad54 molecules were measured by importing raw TIFF images as image stacks into ImageJ. Kymographs were generated by defining a 1-pixel wide region of interest (ROI) along the long axis of individual dsDNA molecules. Data analysis was performed from the kymographs. The start of translocation was defined when the GFP-Rad54 molecule moved >2 pixels. Pauses were defined as momentary stalls in translocation that lasted 2–4 frames. Termination was defined by molecules that did not move for >10 frames. Velocities were calculated using the following formula $[(|Y_f - Y_i|) \times 1000\ \text{bp}/[|X_f - X_i|]) \times \text{frame rate}]$; where Y_i and Y_f correspond to the initial and final pixel position and X_i and X_f correspond to the start and stop time (in seconds). Graphs of individual velocity and distances traveled were plotted in GraphPad Prism 9. We tested several models to fit the data, including a Gaussian and Lognormal distribution. We fit data to a Sum of two Gaussians and a Sum of three Gaussians. These are also types of fits for normal distribution and assumes the presence of two or three normally distributed populations within a data set. The best fit for WT was a Sum of two Gaussians, which was used to analyze the other variants of Rad54 too. We also used this model to fit the distance travelled data. The selection of homologous sequence was performed by measuring the position of GFP-Rad54 and 90-mer Atto647N after 15 min. The probability of all bound sequences was then calculated and plotted. A non-homologous piece of DNA was subjected to the same experiments and analyzed as a negative control. Determination of homology search type was performed by visual inspection of kymographs for evidence of translocation before stabilization at the homologous site.

Single molecule analysis of RPA

Analysis of RPA was performed by visually inspecting kymographs for RPA-mCherry signal that colocalized with

GFP-Rad54 and Atto647N-ssDNA. The association time for RPA was determined by measuring the number of frames it took for RPA to colocalize with GFP-Rad54 and Atto647N-ssDNA. This number was converted to seconds, and then populations were compared. For lifetime measurements, the number of frames with a detectable RPA signal was scored and converted to seconds. This was then plotted on an exponential decay curve to determine the percentage dissociation. The dissociation rate was not used because the curves did not terminate at the same point. Instead, we analyzed the percentage of RPA molecules that did not dissociate within the time frame of the experiment. The estimated number of RPA molecules was determined as follows. First, the peak intensity for an RPA binding event was calculated. Next, a global background signal was then subtracted from the intensity and then divided by the intensity of a single mCherry fluorophore, which has been calculated for this microscope. This yielded an estimated number of RPA molecules. The RPA binding footprint on ssDNA was then used to estimate the overall size of the strand separation.

Multiple sequence alignment of Rad54

Representative RAD54L protein sequences were obtained from UniProt (57) and aligned in Jalview (2.11.3.2) (58) using MUSCLE with default settings (Figure 1B) (for complete alignment, see Supplemental File 1) (59). RAD54L from *Homo sapiens* (UniProt ID: Q92698) was also used to query the non-redundant database of Eukaryotic organisms (Taxonomic ID: 2759) using BLASTp (v. 2.15.0) (4), and the top 1000 hits with an *E*-value <0.05 were aligned in Jalview (2.11.3.2) (60) using MUSCLE with default settings (Supplemental File 1). Only nine (9/1000) hits lacked one of the conserved residues (Arg, Tyr, Asp); eight are additional isoforms of hits containing the complete triad. The last sequence (EHH14742.1) lacks the Asp residue and is from *Macaca mulatta*, which encodes a second Rad54-like protein (UniProt ID: F7BLY5) that contains all three residues (see Figure 1B).

Results

A primary goal of our study was to identify the reduction of function alleles in Rad54. To do this, we initially surveyed the COSMIC database (61). This is a repository for amino acid substitutions identified in human cancers. In selecting residues to mutate, we did not assign a cut-off for the number of cancers the amino acid substitutions were found in or define whether it was a driver or passenger mutation (Supplementary Figure S1A). We also confirmed that the identified residues were conserved across all eukaryotes. In total, we identified 60 amino acid substitutions in Rad54 that fit these criteria. We initially mutated thirteen residues in *S. cerevisiae RAD54* (Supplementary Table S3, which includes equivalent human amino acid) to test the complementation of sensitivity to methylmethanesulfonate (MMS) in *rad54Δ* strains. We chose MMS because there is a well-defined and strong sensitivity phenotype in *rad54Δ* stains, and this would allow us to determine if any of these mutations complement the *rad54Δ* phenotype. Yeast RAD54 shares 48% sequence identity with its human ortholog RAD54L (62), and it has been previously shown that hRAD54L can partially complement the MMS sensitivity phenotype in *S. cerevisiae* (62).

Four amino acid substitutions failed to complement fully, *rad54P43S*, *rad54P43L*, *rad54R272Q* and *rad54E381K* (Supplementary Figure S1B). While the substitution of proline at position 43 was interesting, we did not pursue this residue further because other mutations at this site were not sensitive to MMS. Likewise, the *rad54E381K* allele is a complete loss of function. Based on the *Danio rerio* crystal structure, this mutant likely disrupts an essential alpha helix within one of the RecA lobes (Supplementary Figure S2A, B). This left the *rad54R272Q* allele as a potential reduction of function allele that satisfied our criteria. Interestingly, this mutation has been identified in different malignant melanoma samples, and additional amino acid substitutions were identified in the COSMIC database. These included thyroid (R→L), as well as bladder, brain, and cervical cancer (R→W). We did not test these mutations directly, but the incidence of multiple variants at this site suggests a critical interaction (61).

The Rad54R272 residue is in the ATPase core of the Rad54 structure, and we were able to evaluate the position of this residue in the existing *D. rerio* structure (63) and an Alphafold2 generated structure of the *S. cerevisiae* and *H. sapiens* RAD54 proteins (Supplementary Figure S3A,B). We performed structural superposition of *S. cerevisiae* and *H. sapiens* RAD54 and they fit with and RMSD of 1.05 (Supplementary Figure S3A,B,C). Likewise, we superimposed *S. cerevisiae* Rad54 with *D. rerio* RAD54 (PDB: 1Z3I) and they aligned with a RMSD of 0.91 (Supplementary Figure S3C). Importantly, in these structure superpositions R272, or equivalent formed a cross RecA lobe interaction with residues Y562, or equivalent and D769 or equivalent (Figure 1A,B and Supplementary Figure S3C). Interestingly, the D769 residue was also identified in the COSMIC database as a D769H variant in breast cancer. We also evaluated the conservation of these three residues and found that all three were conserved in all eukaryotes, with an exception. In *Arabidopsis thaliana*, the tyrosine residue was changed to a histidine (Figure 1C and Supplemental File 1). This suggests that this tripartite interaction is conserved in eukaryotes and is likely fundamental to Rad54 biology and genome maintenance. We hypothesized that the R272Q mutation partially reduced function due to a loss of the charge interaction with the D769 mutation. However, this substitution could also potentially maintain a π-stacking interaction with the Y562 residue. If this were true, we would expect a further reduction of function if the R272 site was mutated to alanine.

We generated additional alleles including *rad54R272A*, *rad54Y562A*, *rad54D769H* and *rad54D769A* (Figure 1D). We tested these alleles for MMS sensitivity and found that, as expected, the *rad54R272A* allele was more MMS sensitive than the *rad54R272Q* allele (Figure 1D). Likewise, we observed that the *rad54D769H*, *rad54D769A* and *rad54Y562A* alleles had increased MMS sensitivity but were not as sensitive as the rad54R272Q and *rad54R272A* substitutions (Figure 1D). From this, we conclude that this interaction is required for fully functional Rad54, and we propose that this interaction is important for latching the two RecA lobes. We will refer to this interaction as the Rad54 latch motif. To further validate this hypothesis, we integrated the *rad54R272Q* and *rad54R272A* alleles into the genome and tested the complementation of the MMS sensitivity phenotype. We found that, as with the plasmid-based complementation, integration resulted in strains that were sensitive to MMS (Supplementary Figure S4A). From these results, we conclude that amino acid

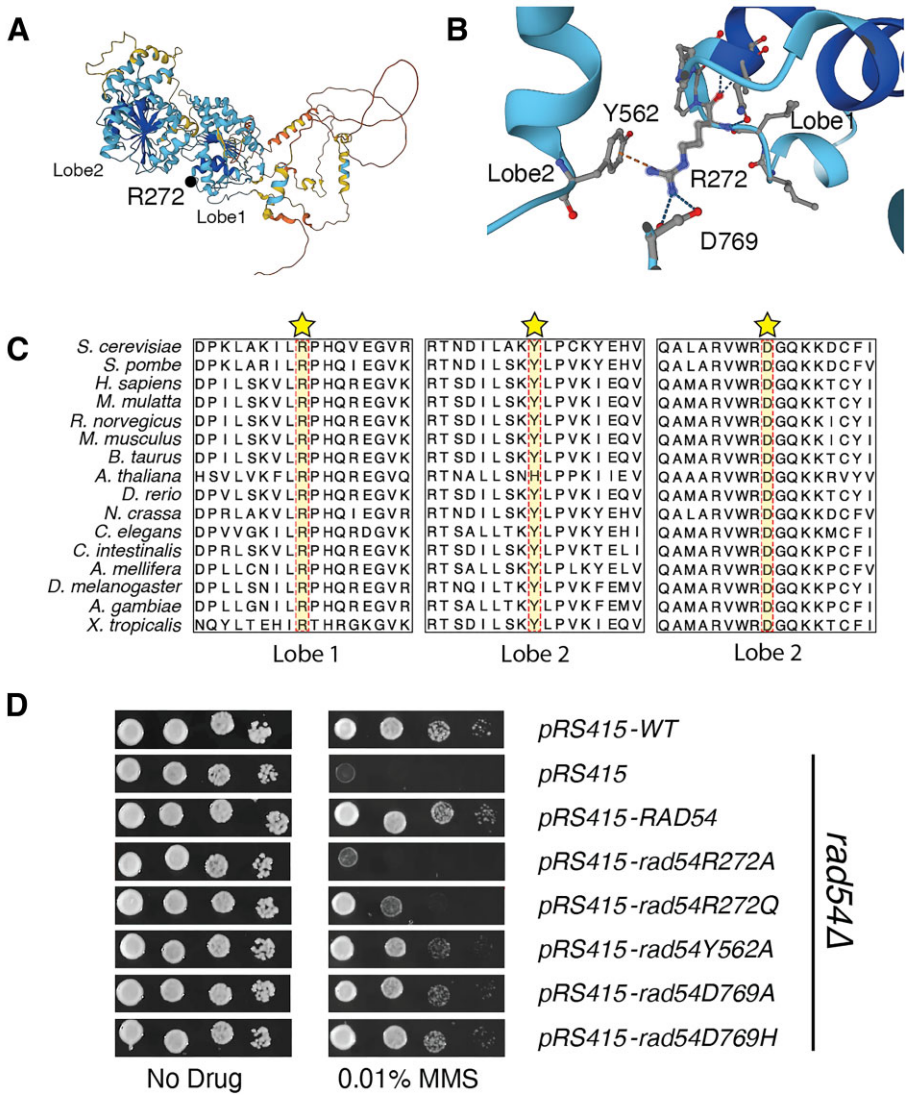

Figure 1. Disruption in the connection between Rad54 lobes leads to increased MMS sensitivity. (**A**) Alphafold2 structure of yeast Rad54. The protein is colored corresponding to the pLDDT format. A black dot illustrates the site of mutation. (**B**) Expanded view within Rad54 that corresponds to a motif that bridges the two RecA lobes. The R272 and D769 residues were mutated in the COSMIC database. (**C**) Three regions of an amino acid sequence alignment of several eukaryotic Rad54 proteins showing the conservation of the R272, Y562 and D769 residues. Protein sequences were obtained from Uniprot and aligned in Jalview (2.11.3.2) using MUSCLE with default settings. (**D**) Yeast complementation assay to evaluate Rad54 mutants for their ability to restore resistance to MMS. Alleles tested includes *RAD54*, *rad54R272A*, *rad54R272Q*, *rad54Y562A*, *rad54D769A* and *rad54D769H*.

substitutions in this region of Rad54 result in a reduction of function.

Overexpression of Rad51 is generally toxic to cells and can have two related yet distinct consequences. If levels of Rad51 are elevated during HR-mediated repair, it can cause increases in CO outcomes and general genetic exchanges between chromosomes (64). These effects are considered on-pathway because they occur during genetic exchange. However, without damage, excessive Rad51 can indiscriminately bind to dsDNA and disrupt the proper segregation of chromosomes (41,42). This binding is considered off-pathway because it occurs in the absence of damage. It is likely that during normal HR, there is crosstalk between these pathways, and regulation of Rad51 in this context is partly controlled by Rad54 and its closely related paralog Rdh54. Because Rad54 can aid in controlling Rad51 off-pathway binding, Rad51 overexpression is partially toxic in *rad54Δ* cells. To determine if the latch mutations were also deficient in controlling off-pathway Rad51 binding, we tested whether the Rad51 overexpression phenotype in the *rad54Δ* was complemented in the *rad54R272Q* and *rad54R272A* strains. We found that the *rad54R272Q* and *rad54R272A* strains were able to complement the sensitivity caused by Rad51 overexpression observed in the *rad54Δ* strains (Supplementary Figure S4B). From this experiment, we conclude that these mutations in Rad54 likely can remove Rad51 from dsDNA under non-damage conditions and are potentially separation of function mutations.

Mutations in the Rad54 latch reduce translocation efficiency on dsDNA

To test our hypothesis that these amino acid substitutions resulted in a reduced Rad54 translocation rate, we proceeded with biochemical characterization of the Rad54R272Q and Rad54R272A. The purified mutant proteins had similar multimerization behavior to WT-Rad54 as measured by size

exclusion chromatography (Supplementary Figure S5A–C). They bound to dsDNA as efficiently as WT (Supplementary Figure S6A) but exhibited reduced ATP hydrolysis activity (Supplementary Figure S6B, D). However, their ATPase was still stimulated by adding Rad51 (Supplementary Figure S6C,D). This indicates that they are defective in hydrolysis but still interact with Rad51. Next, we used DNA curtains (55,56) to characterize the activity of WT-Rad54, Rad54R272Q, and Rad54R272A. This single molecule approach allows us to measure the DNA binding, velocity, and translocation distance of Rad54 molecules (Supplementary Figures S7A–D and S8A–C).

We initially characterized the ability of Rad54, Rad54R272Q and Rad54R272A to bind dsDNA by quantifying the number of binding events per dsDNA and the intensity of GFP associated with each binding event (Supplementary Figure S7B–D). We did not observe a difference in the number of DNA binding events per DNA molecule for WT-Rad54, Rad54R272Q or Rad54R272A for either Rad54 alone or in the context of the Rad51/Rad54 presynaptic complex (PSC) (see below). However, there were differences in the GFP intensities for Rad54 binding alone between the WT-Rad54, Rad54R272Q and Rad54R272A variants. This difference was not observed in the context of the Rad51/54 PSC (Supplementary Figure S7D). Next, we measured the translocation velocity of WT-Rad54 and found it to be 65 ± 67 bp/s with a mean track length of 3.7 ± 2.5 kb (Supplementary Figure S8A–C). These values are consistent with previous observations (8). However, we could not measure Rad54R272Q or Rad54R272A as they did not move far enough to calculate an accurate velocity (Supplementary Figure S8A–C). From these data, we conclude that Rad54R272Q and Rad54R272A have reduced translocation capacity.

We next evaluated the activity of Rad54R272Q and Rad54R272A in their ability to support Rad51 sequence alignment during the homology search. We have developed an *in vitro* single molecule assay to monitor Rad54 activity during the homology search and DNA alignment step of HR using DNA curtains (Figure 2A). In this experiment, Rad51 is preincubated with a 90 nt ssDNA oligo labeled with Atto647N. This allows the formation of short recombinase filaments or pre-synaptic complexes (PSCs). These structures are mixed with GFP-Rad54 and RPA-mCherry and flowed onto a preformed DNA curtain made from lambda dsDNA. This configuration allows direct observation of the Rad51-PSC bound by Rad54 as it searches for a homologous DNA sequence. In this experiment, we can measure the velocity and distance traveled by the Rad51/54-PSC. When using labeled RPA, we can also measure the association of RPA with the PSC, the time to RPA association, and the RPA binding lifetime. Finally, when a homologous sequence to the lambda DNA is used, we can also measure the probability of identifying the homologous sequences (Figure 2B). These measurements allow us to directly monitor the *in vitro* homology search.

For WT-Rad54, we measured the velocities of two unique populations. The faster of the two populations had a mean velocity of 394 ± 183 bp/s, and the slower one had a mean velocity of 114.3 ± 73 bp/s (Figure 2E). Rad54R272Q and Rad54R272A had only a single population of velocities with a mean of 42.42 ± 23.73 bp/s and 25.7 ± 15.32 bp/s, respectively (Figure 2C–E). We also measured the mean distance traveled by a unique Rad51/54-PSC before stopping or dissociating. We also observed two populations for distance travelled by WT. These populations had mean distance travelled of 4.1 ± 0.9 and 6.2 ± 1.9 kb, respectively (Figure 2F). We also observed two populations within the Rad54R272Q data, however we were only able to accurately fit the first of these populations which had a distance travelled of 4.1 ± 1.7 kb and was the same as WT. The second population was likely not measurable because there were fewer total molecules in this population than in WT. Finally, the Rad54R272A had a single population of 3.4 ± 1.3 kb, and completely lacked a second population (Figure 2F). From these data there is only a slight difference in the distance the PSC translocated when mutating the latch domain. The difference derives from the reduction and loss of a second population of longer travelling molecules. From these data we conclude that mutations in the Rad54 latch domain have a greater impact on translocation rate than distance travelled. Within these data sets we also observed two populations of molecules in the WT, this changed when mutating the latch domain. At this point we cannot determine the difference between these populations and choose not to interpret the meaning of these two populations because we don't know what each of them represents. We can conclude from these data that mutations in the latch domain cause defects in Rad54 activity when incorporated into the PSC.

Rad54 mutations impair donor DNA strand opening

It has previously been shown that as Rad51/54 PSCs move along DNA, they can recruit RPA. This is not through protein-protein interaction and likely results from the generation of locally underwound DNA behind translocation and overwound DNA ahead of translocation (8,15) (Figure 3A). We evaluated how Rad54R272Q and Rad54R272A affected RPA dynamics during PSC translocation (Figure 3B). We estimated the number of RPA-mCherry molecules associated with translocating PSCs by comparing their overall intensities with known intensities from individual photobleaching experiments (65). This analysis measured the mean number of RPA molecules bound to PSCs at 2.5 ± 1.5 (Figure 3C). This value was like previously reported values (8). In contrast, Rad54R272Q and Rad54R272A had RPA values of 2.13 ± 1.2 and 1.75 ± 1.3, respectively (Figure 3C). These values represent a significant difference from WT. If we quantize the amount of RPA, then WT-Rad54 will likely have 2–3 molecules of RPA bound, representing underwound DNA of 60–90 nt. In contrast, the mutant versions of Rad54 are likely to have 1–2 molecules of RPA, suggesting an underwound region of 30–60 nt. From these data, we conclude that the Rad54 substitutions have reduced strand opening activity.

Next, we evaluated the kinetics of RPA's association with PSC. We measured the time it took to observe RPA associating with the PSC after it bound to the dsDNA. We found that the median association time for WT-Rad54 was 0.14 min (Figure 3D, E). In contrast, the Rad54R272Q and Rad54R272A mutants had median association values of 0.6 and 0.73 min, respectively (Figure 3D, E). These data likely reflect that these Rad54 mutants are delayed in their ability to generate underwound DNA. We also measured the percentage of RPA molecules that localized/associated with PSCs but dissociated after binding from the complex. From this, we could infer the stability of the underwound DNA and RPA binding site. This was a better overall measure of stability than the decay rate because, in many cases, the RPA did not dissociate within the

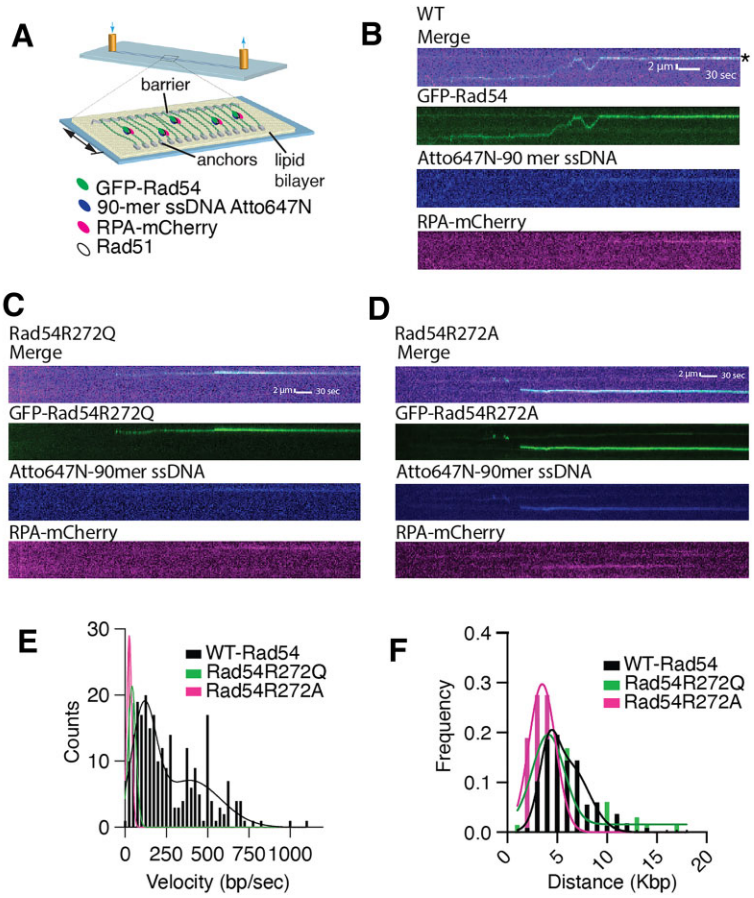

Figure 2. Disruption of the Rad54 latch reduces translocation velocity of the Rad51/54 PSCs. (**A**) Cartoon diagram illustrating DNA curtains experiment to monitor Rad51/54 PSCs during the homology search step of HR. (**B**) Representative Kymograph illustrates GFP-Rad54 (Green) as part of the Rad51/54-PSC translocation along DNA in search of homology. The recipient 90-mer ssDNA Atto647N (middle) is labeled in blue, and RPA-mCherry (bottom) is included in the reaction (magenta). The Asterix denotes the sites of homology. (**C**) Kymographs for Rad54R272Q-PSCs with Merge, GFP-Rad54R272Q, Atto647N-90mer ssDNA, RPA-mCherry. (**D**) Kymographs for Rad54R272A-PSCs with Merge, GFP-Rad54R272A, Atto647N-90mer ssDNA, RPA-mCherry. (**E**) Distributions of measured velocities for WT-Rad54 ($N = 248$), Rad54R272Q ($N = 65$) and Rad54R272A ($N = 58$). A sum of two Gaussian distributions fits the data of WT-Rad54. (**F**) Distributions of measured translocation distances for WT-Rad54 ($N = 248$), Rad54R272Q ($N = 65$) and Rad54R272A ($N = 58$). A sum of two Gaussian distributions fits the data.

viewing window of the experiment. For WT-Rad54, we found that 55% of RPA molecules dissociated after binding (Figure 3D, F). In contrast, 69% of RPA molecules dissociated after binding in the case of the Rad54R272Q mutant, and 84% of RPA molecules dissociated in the case of the Rad54R272A mutant (Figure 3D, F). Because the overall percentage of dissociated RPA molecules is lower in the case of the WT-Rad54, it suggests that the RPA binding sites are more stable. These data indicate that these Rad54 substitutions have a reduced ability to generate and stabilize strand-separated DNA.

A reduction in motor function alters DNA sequence alignment

Identification of the correct DNA sequence during the homology search can occur through 1D or 3D movement of the PSC (8,10). In our assay, we can identify successful searches that have occurred through 1D movement by determining if there is movement along the DNA before sequence recognition (Figure 4A). We can also observe sequence recognition events that appear to occur through direct binding from the solution (Figure 4A). We interpret these recognition events to mean the sequence has been identified by 3D movement. We cannot exclusively rule out a translocation event that is faster or shorter than the resolution of our experiment. However, we are confident these represent unique search outcomes in our experiment and can quantify them as such. From these assumptions, we can determine the efficiency of DNA alignment through both 1D and 3D movement.

We first calculated the global frequency of DNA sequence alignment by monitoring the Rad51/54-PSC dwelling at the correct region of homology versus all possible binding sites after fifteen min of observation. These values are compared to a non-homologous piece of DNA to determine whether the homologous site is enriched. In these experiments, the WT-Rad54 is aligned with the homologous site with a probability of 0.165. This is 5.75-fold higher than the measured probability of 0.0285 for non-homologous DNA and 7.5-fold higher than the mean probability for all non-homologous sites, 0.022 (Figure 4B,C and Supplementary Figure S9A–D). In contrast, the Rad54R272Q and Rad54R272A had a probability of 0.11 and 0.09, respectively. This represented a 1.5-fold and 1.8-fold reduction from WT-Rad54, respectively (Figure 4B, C and Supplementary Figure S9A–D). From these data, we conclude that the Rad54 mutations impair DNA sequence alignment, likely due to a reduction in motor function.

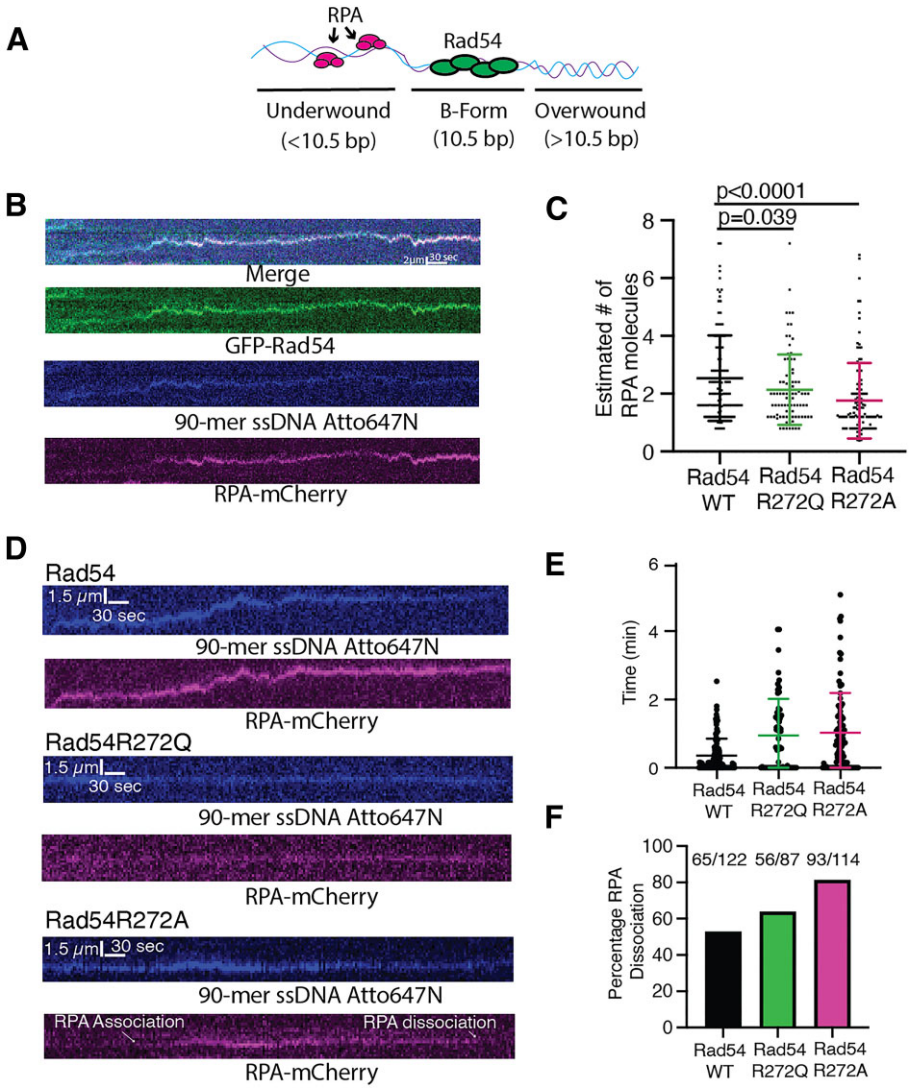

Figure 3. Mutations in Rad54 influence RPA dynamics on the PSC. (**A**) Cartoon schematic illustrating the proposed model for Rad54 movement on dsDNA. Movement creates underwound DNA behind and overwound DNA ahead. (**B**) Representative kymograph illustrating co-translocation of GFP-Rad54 (green), 90-mer ssDNA-Atto647N (blue), and RPA-mCherry (magenta). (**C**) Dot plot representing the estimated number of RPA molecules based on photobleaching measurements for an individual step size for WT-Rad54 ($N = 119$), Rad54R272Q ($N = 87$) (green) and Rad54R272A ($N = 114$) (magenta). The cross and error bars represent the mean and standard deviations of the data. (**D**) Representative kymographs for WT (top), Rad54R272Q (middle) and Rad54R272A (bottom). The 90-mer ssDNA-Atto647N from the PSC (blue) and RPA-mCherry (magenta) are shown. (**E**) Dot plot representing the time it takes for RPA to associate with Rad51/54-PSCs that are bound to dsDNA for WT-Rad54 ($N = 108$) (black), Rad54R272Q ($N = 60$) (green), Rad54R272A ($N = 95$) (magenta). The cross and error bars represent the mean and standard deviation of the data. (**F**) Bar graph representing the fraction of RPA molecules that bound to the PSC but then dissociated before the end of the experiment for WT-Rad54 ($N = 122$) (black), Rad54R272Q ($N = 87$) (green) and Rad54R272A ($N = 114$) (magenta).

Next, we evaluated the population of molecules at the target site that aligned via long range (>2 kb) 1D movement versus 3D movement. For WT-Rad54, 66% (32/48) were aligned by 1D movement, and 34% (16/48) were aligned by 3D movement (Figure 4D). By comparison, Rad54R272Q aligned DNA by 1D movement 33% (4/12), and Rad54R272A aligned DNA by 1D movement 22% (6/27) of the time. These data suggest that DNA sequence alignment is reduced in these Rad54 mutations and that there is a change in the mechanism used to align DNA. We also measured the number of PSCs aligned with the homologous sequence at any point during the experiment for longer than twenty seconds but then dissociated. In the case of WT-Rad54, this number was 18% (11/59) (Figure 4E). For Rad54R272Q and Rad54R272A, it was 29% (5/17) and 33% (13/40), respectively. From these data, we conclude that a reduction in the rate of Rad54 translocation leads to a diminished capacity to align DNA stably.

Rad54 mutants require longer stretches of homology to form stable D-loops

Our single molecule analysis indicates that Rad54R272Q and Rad54R272A have reduced capacity to translocate on DNA, align DNA, and stabilize strand opening events. These data suggest that these proteins should be deficient in D-loop formation. To test this question, we used an *in vitro* D-loop formation assay (Figure 5A). This assay is based on the pairing and stabilization of short D-loops using the pUC19 plasmid as a substrate. We performed the experiments with 65-, 90- and 130-nt of homology. Each homologous ssDNA contained

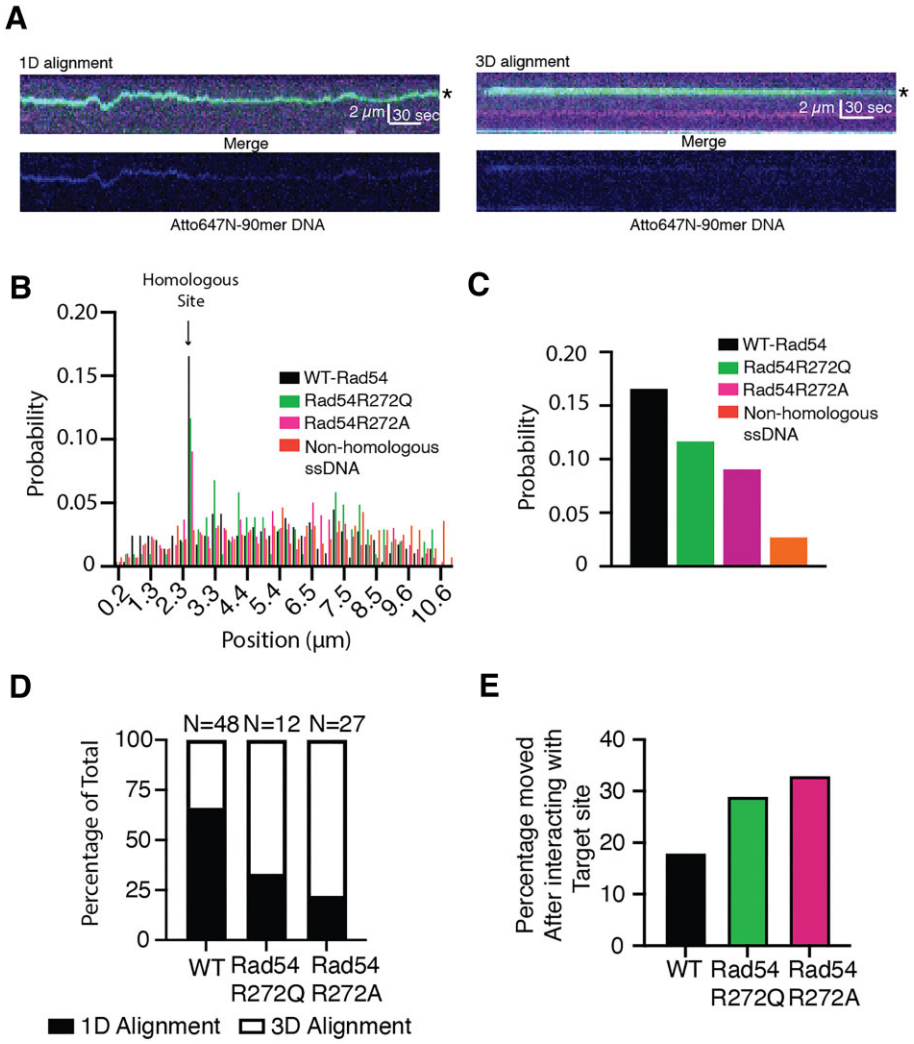

Figure 4. Reduced Rad54 activity alters the efficiency of DNA sequence alignment. (**A**) Representative kymographs illustrating the alignment of the homologous sequence by 1D movement (left) and 3D movement (right). The kymographs represent a merged three-color image (top) of GFP-Rad54 (green), RPA-mCherry (magenta), and 90-mer ssDNA Atto647N (Blue) and an individual image of the Atto647N-90-mer (bottom). A star denotes the site of homology. (**B**) Graph representing the binding probability distribution of PSCs across lambda DNA after 15 min. An arrow marks the site of homology. The data are for Rad51/54-PSCs consisting of WT-Rad54 ($N = 290$) (black), Rad54R272Q ($N = 103$) (Green), and Rad54R272A ($N = 298$) (magenta). Non-homologous sequence ($N = 280$) (orange). (**C**) The expanded view of the graph in (B) represents only the homologous site. (**D**) Graph representing the percentage of sequence alignment events that occur via 1D movement versus 3D movement for WT-Rad54, Rad54R272Q and Rad54R272A. (**E**) Bar graph illustrating the number of PSCs that bind to the target site but then move after dwelling for at least 10 s.

a 25 nt non-homologous stretch at the 5′ end of the DNA that was annealed with a 25 nt oligo labeled with Atto647N (Figure 5A).

We first measured the 65-mer homologous sequence and found that WT-Rad54 could promote stable D-loop formation. In contrast, we failed to observe measurable D-loop formation with Rad54R272Q and Rad54R272A (Figure 5B, C). Next, we measured 90 nt of sequence homology. As with the 65-mer, the WT-Rad54 promoted the formation of stable D-loops. For RadR272Q in some experiments ($n = 2/5$), we observed stable D-loop formation with a 5-fold reduced efficiency relative to WT-Rad54 (Figure 5D, E). For the Rad54R272A mutant, we observed measurable D-loop formation in fewer ($n = 1/5$) experiments, and in this experiment, there was a 6-fold reduction relative to WT-Rad54. When using a 130 nt homology, we were able to see consistent D-loop formation for both the Rad54R272Q ($n = 3/3$) and the Rad54R272A mutations ($n = 4/4$) (Figure 5F,G). However, both mutants formed D-loops with reduced efficiency, 2.3-fold for Rad54R272Q and 3.5-fold for Rad54R272A, relative to WT-Rad54. From these experiments, we conclude that the Rad54R272Q and Rad54R272A proteins have reduced capacity to form stable D-loops and that longer tracts of homology can begin to alleviate the reduction of this activity. Because more extended regions of homology are required for stable D-loop formation with the Rad54 latch mutations, this is consistent with the role of the Rad54 in stabilizing shorter early pairing events.

Reduction in Rad54 function leads to increases in crossover outcomes

The HR reaction proceeds through a series of intermediates determining whether DNA sequence information is passed between donor and recipient DNA molecules. These intermediates primarily depend on the capture of the second DNA end.

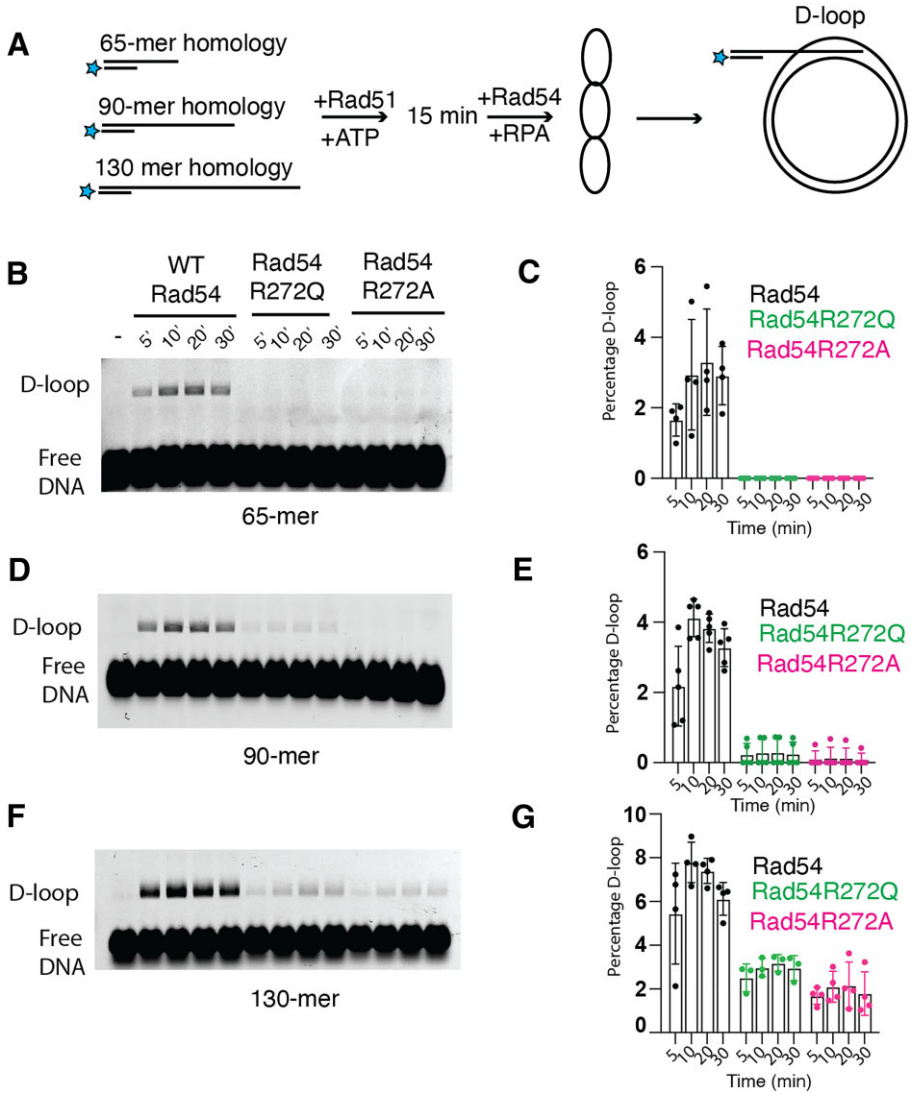

Figure 5. Rad54 mutants have a diminished ability to form D-loops *in vitro*. (**A**) Cartoon diagram illustrating experiment to measure WT-Rad54, Rad54R272Q and Rad54R272A activity for D-loop formation with different lengths of homology. (**B**) Representative gel illustrating D-loop formation for WT-Rad54, Rad54R272Q and Rad54R272A with a 65-mer of homology to the pUC19 plasmid. (**C**) The bar graph quantifies the D-loop formation percentage for WT-Rad54, Rad54R272Q, and Rad54R272A. The error bars represent the standard deviation of 4 independent experiments. (**D**) Representative gel illustrating D-loop formation for WT-Rad54, Rad54R272Q and Rad54R272A with a 90-mer of homology to the pUC19 plasmid. (**E**) The bar graph quantifies the percentage of D-loop formation for WT-Rad54, Rad54R272Q and Rad54R272A. The error bars represent the standard deviation of 5 independent experiments. (**F**) Representative gel illustrating D-loop formation for WT-Rad54, Rad54R272Q and Rad54R272A with a 130-mer of homology to the pUC19 plasmid. (**G**) The bar graph quantifies the D-loop formation percentage for WT-Rad54, Rad54R272Q and Rad54R272A. The error bars represent the standard deviation of 3–4 independent experiments.

For example, if the D-loop is disrupted, the recipient DNA is annealed to the second broken end and used as a repair template as part of the SDSA pathway. This results in non-crossover (NCO) outcomes. If the D-loop is not disrupted and the non-template strand captures the second end, a double Holliday junction (dHJ) can form. This structure can result in crossover (CO) or NCO outcomes. If the second end is not located or does not exist, break induced reapplication (BIR) can occur, a mutagenic long-range replication event that can result in loss-of-heterozygosity (LOH) outcomes.

Rad54 is believed to promote NCO outcomes (66,67), which protects genomic integrity by preventing excessive sequence exchange between donor and recipient DNA molecules. Previous reports have shown that overexpression of *RAD54K341R* has a dominant negative effect on WT strain, causing increases in CO outcomes in diploid yeast (46). This could be due to the disruption of Rad54 ATPase activity, as this motor functions as a multimer (8,48). We hypothesized that *rad54R272Q* and *rad54R272A* mutants may have similar phenotypes and could result in higher CO levels.

We used a genetic reporter assay that monitors outcomes of allelic exchange between homologous chromosomes (27,68). Strains used in this assay have ade2 (ade2-I and ade2-n) heteroalleles located on chromosome XV. One of these alleles has an I-Sce1 cleavage site (ade2-I), and the other has a disrupted reading frame toward the start of the gene (ade2-n). Double strand breaks can be induced by the expression of the I-Sce1 nuclease under the control of a galactose inducible promoter. In this experiment, both sister chromatids are cut, which results in the ade2-n gene on the homologous chromosome

being used as a repair template. This results in gene conversion events. Short tract gene conversion events, <1 kb, result in recovery of an active *ADE2* gene and white colonies. Long tract gene conversion outcomes, >1 kb, result in the conversion of the ade2-I to ade2-n, which maintains an inactive copy of the gene. Each sister chromatid can undergo gene conversion through either long or short-tract repair. If each is repaired by the same type, then the colony is either red or white. However, if one sister is fixed by short tract and the other by long, the colonies can be red/white sectored. These colonies are most important for inferring recombination outcomes because they have undergone division before plating. It should be noted that cutting both sister chromatids simultaneously is unlikely to occur naturally, and this assay is being used as a model to understand how functional disruption of Rad54 could relate to outcomes in a recombination reaction.

Each homologous chromosome contains a different antibiotic marker to determine the outcome of a recombination reaction. NCO outcomes occur when there is no change in the segregation pattern of the antibiotic markers because the chromosomes remain heterozygous. CO outcomes can be inferred when each part of a sectored colony is sensitive to different antibiotics. This occurs because antibiotic markers have switched chromosomes, and chromosome VX in this colony is now homozygous for one antibiotic marker. This loss-of-heterozygosity (LOH) event can occur with long-track or short-track repair. Another outcome that can be determined from this assay is break-induced replication (BIR). This can be inferred in a sectored colony when a red sector is resistant to both antibiotics, and the white sector is only resistant to one. This represents a LOH event in which a long-track repair event has copied the antibiotic marker during repair (Figure 6A, B) (69). This assay also contains markers to report on chromosome loss. We have previously used this assay and found that *rad54Δ/rad54Δ* strains are severely defective in this assay and result in limited recombination (27).

We compared the *rad54R272Q* and *rad54R272A* alleles to the WT for their ability to promote recombination (Supplementary Figure S10A, B and Supplementary Tables S4-- S6). In contrast to the *rad54Δ*, latch mutation strains promoted viable recombination outcomes that had similar viability to WT (Supplementary Figure S10A,B). For sectored recombinants, WT resulted in 50.4 ± 2.7% CO (Figure 6C). In contrast, the *rad54R272Q* substitution resulted in 61 ± 2.8% CO, and the *rad54R272A* substitution resulted in 64 ± 4.5% CO (Figure 6C and Supplementary Tables S4–S6). The *rad54R272A* allele had slightly increased chromosome loss, which could account for the difference from the *rad54R272Q* allele (Supplementary Table S4-S6). For solid red recombinants, WT strains only resulted in CO outcomes 13.2 ± 4.6% of the time. The *rad54R272Q* and *rad54R272A* alleles displayed increased CO outcomes with 30.3 ± 10% and 28.3 ± 9%, respectively (Figure 6D and Supplementary Table S4-S6). When we combined the total recombinant population, we observed that 40 ± 1.1% of recombinants resulted in CO outcomes in WT. In the rad54R272Q and rad54R272A mutants these numbers were 50.4 ± 4.0% ($P = 0.0003$) and 56.3 ± 3.4% ($P < 0.0001$) respectively (Figure 6E). Together, these data suggest that reducing Rad54 activity increases CO outcomes. We also measured BIR outcomes and observed a 2-fold reduction in the BIR observed in the *rad54R272Q* and *rad54R272A* relative to WT (Supplementary Figure S10C–E). This is consistent with previous reports that the rate of strand invasion may affect BIR outcomes (27), and these data suggested that *rad54R272Q* and *rad54R272A* may promote strand invasion at reduced rates.

Rdh54 is a paralog of Rad54 which is also conserved in higher eukaryotes as the ortholog RAD54B. It has been shown that Rad54 and Rdh54 are partially redundant in function and work to control Rad51 both in what is considered on-pathway and off-pathway activities (12,41,42,70–72). On-pathway regulation occurs during DSBR, where these motors control strand invasion and D-loop metabolism. Off-pathway regulation occurs when these motors prevent the accumulation of excess Rad51 on chromosomal DNA. Thus, preventing mis-segregation during cell division. Mutations in the latch region of Rad54 led to increased CO outcomes during allelic recombination. We hypothesized this could be due to a reduced rate of strand invasion, which indirectly leads to longer-end resection products and gene conversion tracts associated with crossovers. If this is the case, we expect the deletion of Rdh54 to cause a further increase in CO outcomes through one of two possible mechanisms. Directly by controlling the length of strand invasion products by regulating Rad54 during D-loop formation (14) or indirectly by regulating *in vivo* pools of Rad51(42,70).

We generated *rdh54Δ* strains in the *rad54R272Q/A* backgrounds. As has previously been reported (27), there was little impact on changes in CO in the *rdh54Δ* strains (Figure 6C,D). We also observed a significant increase in BIR outcomes (Figure 6E). When we tested the *rad54R272Q rdh54Δ* double mutant, there was an increase in total CO events to 57.6 ± 3.6%. This was larger than the *rad54R272Q* strain (Figure 6C–E) and was consistent with the hypothesis that deletion of *RDH54* may result in longer, more stable strand invasion intermediates. We cannot determine if this is due to direct or indirect effects. An increase in chromosome loss was also observed in the double mutant (Supplementary Table S5). This would be consistent with disrupting the off-pathway effects of Rdh54, which may cause an increase in un-regulated Rad51, leading to longer strand invasion intermediates (41,73). However, we cannot say this conclusively. We observed a restoration of BIR outcomes to the WT level (Supplementary Figure S7B–D), which is consistent with a change in the on-pathway rate of strand invasion, which is likely due to an increase in deregulated Rad51 (27). After several attempts, we could not get healthy diploids with the *rad54R272A rdh54Δ* double mutants. This should have been expected, as previous reports have shown that a *rad54Δrdh54Δ* double mutant yields a severe reduction in diploid growth (72,74). These observations are consistent with a strain that has become too defective to support viability in the diploid state, likely due to severe defects in chromosome maintenance. From these data, we conclude that a reduction in Rad54 activity results in increased genetic exchange in the form of CO outcomes.

Discussion

Here, we have identified and characterized the activity of Rad54 reduction of function substitutions that slow down the translocation activity of Rad54. This amino acid site was found in the COSMIC database from multiple cases of malignant melanomas. We further identify this residue as central to the Rad54 latch domain, which is conserved in eukaryotes. Substitutions at this site diminished Rad54 activity, which

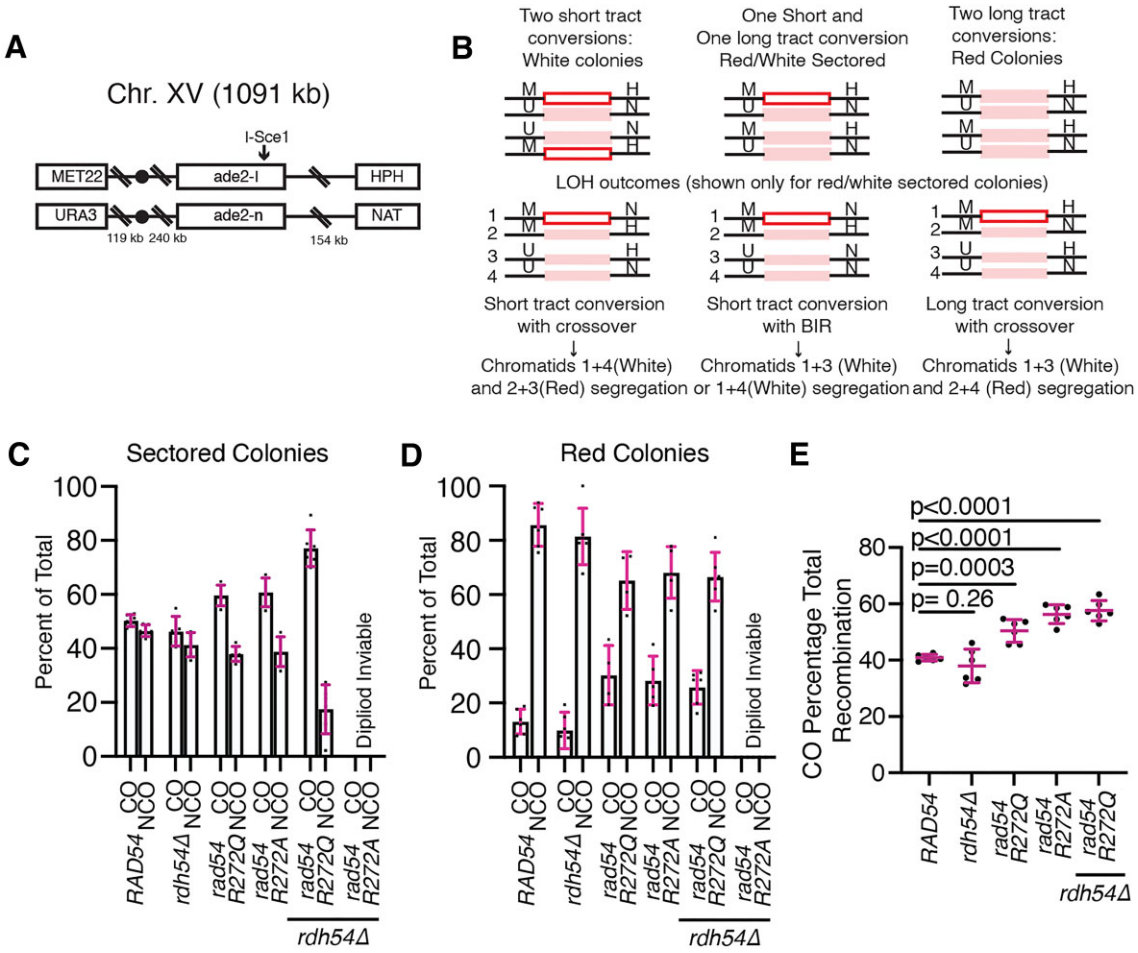

Figure 6. Mutations in Rad54 lead to increased crossover outcomes. (**A**) Schematic diagram illustrating the double strand break reporter construct used in these experiments. (**B**) Schematic diagram illustrating the possible recombination outcomes using this assay. The general outcome from recombination can be inferred from the color of the colony and the antibiotic sensitivity. (**C**) Graph illustrating the CO and NCO outcomes for sectored colonies of WT, *rdh54Δ*, *rad54R272Q*, *rad54R272A*, *rad54R272Q rdh54Δ* and *rad54R272A rdh54Δ*. The error bars represent the standard deviation of six independent experiments. (**D**) Graph illustrating the CO and NCO outcomes ratio for solid red colonies of WT, *rad54R272Q*, *rad54R272A*, *rdh54Δ*, *rad54R272Q rdh54Δ* and *rad54R272A rdh54Δ*. The error bars represent the standard deviation of six independent experiments. (**E**) Graph illustrating crossover outcomes as a percentage of total recombination events for WT, *rad54R272Q*, *rad54R272A*, *rdh54Δ*, *rad54R272Q rdh54Δ* and *rad54R272A rdh54Δ*. The bars represent the mean, and the error bars represent the standard deviation from six independent experiments.

caused the formation of unstable abortive strand invasion intermediates. This leads to an increase in genetic exchange as characterized by CO outcomes. While our study pertains to Rad54 activity, it suggests that factors that promote kinetic regulation of early D-loop intermediates can balance HR outcomes.

Cancer substitutions

We used the COSMIC database to identify amino acid substitutions in Rad54 that, when analyzed, were reduced in function. What we discovered was a near universally conserved three amino acid motif that caused a decrease in Rad54 activity. This latch structure was located on the interface between the two RecA lobes of Rad54, with the R272 residue acting as the lynchpin to tie the lobes together. We hypothesize that this interaction is a charge-charge interaction between R272 and D769 and a π-stacking interaction between Y562 and R272. In the sole example of Rad54, that had a substitution in the latch, *A. thaliana* had a histidine where the tyrosine is found in all other species. We suspect this histidine can still form a stacking interaction with the arginine, conserving this part of the interaction. The D769 residue was also found in the COSMIC database mutated to a histidine.

Rad54 is intrinsically flexible and, like other Snf2 motors, can exist in an open and closed state (75). When bound to dsDNA and ATP, the lobes align, and the motor can translocate along dsDNA. Based on the location of the latch, these residues likely work together to prevent the two RecA lobes from drifting apart as the enzyme resets for the next round of hydrolysis and translocation (76). Disruption of the latch results in defective Rad54 translocation and reduced ATP hydrolysis. The universal conservation of the latch structure and the existence of mutations in human cancers indicate an interaction critical for genome maintenance in all eukaryotes. The consequence of losing this interaction is increased genetic exchange between chromosomes and sensitivity to the genotoxin MMS. While we cannot identify these amino acid substitutions as the cause of malignant melanoma in these patients, it would almost certainly have been an underlying factor in disease progression. While this is a specific case, it suggests that human cancers with low-functioning Rad54 may be prone to genetic exchange, as discussed below. Ultimately, while this may limit Rad54's use as a potential drug target, these results

offer new insight into its use as a diagnostic marker to evaluate the likelihood of genomic rearrangements for specific cancer types.

A major caveat to our study is that we have analyzed these cancer mutations in *S. cerevisiae* strains and proteins. Evolution and experimental evidence would suggest that *S. cerevisiae* and *H. Sapiens* proteins will function the same at the protein/enzyme level. However, we can't exclusively rule out that there are unexpected differences between these homologs. Therefore, our results should be interpreted with caution. It is more likely that there could be differences between how these mutations effect *in vivo* activity of RAD54, as it is probable that yeast and human cells may deploy RAD54 activity in different ways. Future studies to understand differences in cellular use of RAD54 will be necessary to understand the true biological role of this protein in human cancers.

1D translocation based homology search

As part of HR based repair, the homology search occurs through multiple biophysical mechanisms, including 1D/3D diffusion and 1D translocation-based searches (8–10,18,77). The efficiency of 3D diffusive-based mechanisms will scale proportionally with the length of homology and concentration of non-specific competitor DNAs (9). Longer pieces of homology increase the probability of productive contact between the donor and recipient DNA. Rad54 can contribute to the homology search *in vitro* by increasing association with donor DNA (78) and providing a 1D translocation-based search that enhances sequence alignment efficiency (8).

1D translocation along dsDNA is severely compromised in the Rad54R272Q and Rad54R272A mutants. This causes reduced DNA sequence alignment by the Rad51/54-PSC and a diminished ability to form D-loops in bulk. Rad54 latch substitutions failed to create stable D-loop products on short homologous DNA sequences. However, as the size of the homologous sequence increased, we were able to observe the formation of stable D-loops. We interpret this result to mean that Rad54 translocation is important for sequence alignment *in vitro* but may be dispensable for D-loop stabilization. The data supports a model where strand opening, and stabilization are critical features in Rad54 mediated D-loop formation. If translocation were critical in stabilizing D-loop formation, we would have expected the opposite result, and the Rad54R272Q/A substitutions would have formed D-loops on shorter substrates instead of longer. This suggests that the strand-opening activity of Rad54 is critical for D-loop formation (discussed below), which can still function, with reduced efficiency, in the mutated proteins if there are increases in 3D collisions between the recipient and donor DNA.

While the direct contribution of Rad54 translocation to the homology search remains to be defined *in vivo*, the increased efficiency of target selection afforded by motor function may increase repair when the sister chromatid is the preferred template, increasing the kinetics of sequence alignment in a local context. Here, we have identified mutations in Rad54 that may contribute to decreased 1D homology search and strand opening, leading to sensitivity to DNA-damaging agents in cells. Further work will be needed to identify the precise *in vivo* role of Rad54 during the homology search.

Rad54 can use topology to regulate sequence recognition probability

The superhelical density of donor dsDNA can regulate strand invasion and the general HR reaction (79–81). Negative supercoiling of DNA causes strand underwinding characterized as <10.4 bp per turn of the double helix. The underwinding of DNA improves the activity of Rad51-mediated invasion by reducing the energy required to separate DNA strands and make each subsequent triplet pairing event between the donor and recipient DNA. Rad54 can regulate superhelical density by adding twist to DNA, likely generating negative supercoils behind translocation and positive supercoils ahead (15). This activity leads to local DNA melting, as observed by the association of RPA with moving Rad51/54 PSCs (8). Here, we have identified variants in Rad54 that generate shorter and less stable regions of underwound DNA. These lack efficient D-loop formation and are sensitive to the DNA-damaging agent MMS.

Current structural models show that RecA promotes progressive base pairing during strand invasion by separating the donor DNA strands by sequestrating the outgoing strand by Loop 2. This allows additional homology pairing and extends the initial D-loop (82,83). This model predicts that strand pairing occurs over a short distance with the probability of invasion termination occurring once every 15 bp (82,83). This is consistent with observations made on hRAD51 in the post-synaptic state (84), and the Rad51 mechanism is likely similar. These short D-loops may be sufficient to promote repair in bacteria, may be stabilized by the cooperation of multiple short invasion products that accumulate over time, or further extension is facilitated by higher concentrations of RecA required to drive the reaction to completion. However, in eukaryotes, they may be kinetically unstable in the competitive environment of the nucleus or be limited in length by the overall pools of available Rad51 (9). In this case, these pairing events may result in abortive invasion events that fail to extend and form stable D-loop intermediates competent for repair.

We support a model where Rad54 uses ATP hydrolysis to promote topological changes in donor DNA that reduce abortive Rad51 invasions. In this case, strand separation promoted by Rad54 activity will catalyze the expansion of Rad51 invasion products and promote stabilization of shorter Rad51 filaments through further base pairing (Figure 7A, B). The mechanism of catalysis is the generation of underwound DNA, decreasing the probability of termination during each base pairing event. This is likely most important on shorter Rad51 filaments. Overall, this mechanism would increase the rate of HR by ensuring that early homology recognition events are converted to stable D-loop intermediates competent to promote repair.

The reduction of Rad54 biochemical activity increases abortive invasion, ultimately slowing the HR reaction rate (Figure 7A,B). The failure to initiate rapid repair could lead to increased DNA end resection (85,86) and the accumulation of ssDNA within the genome, leading to the potential for complex rearrangements (87,88). Complex chromosomal rearrangements within the genome characterize many human cancers due to defects in DSBR pathways. Re-arrangements can also lead to the development and the evolution of existing tumors (89–92). As discussed below, increases in abortive invasion may cause higher crossover outcomes.

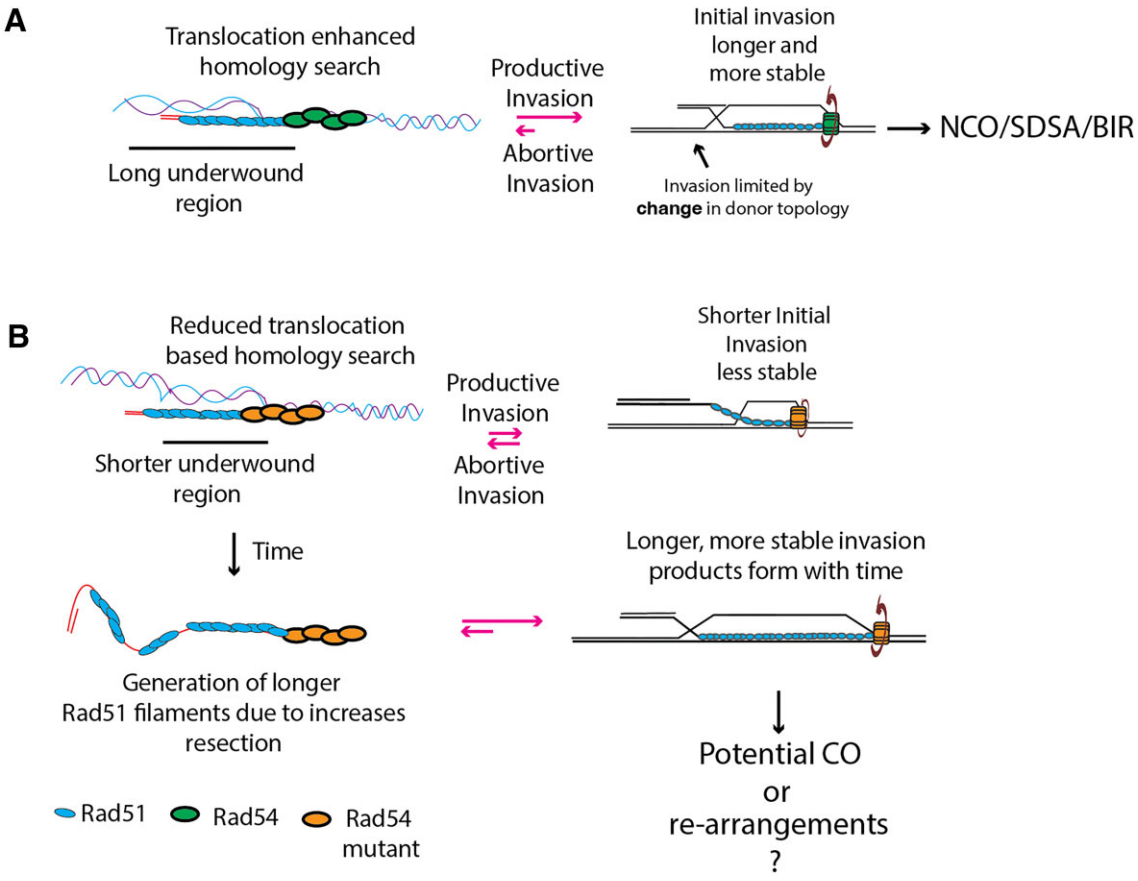

Figure 7. Model for reduction in abortive invasion. (**A**) Schematic diagram illustrating that longer tracts of underwound DNA generated by Rad54 lead to faster invasions and NCO repair or SDSA. (**B**) Mutant versions of Rad54 lack general translocation activity and produce shorter regions of underwound DNA, leading to less stable invasion products. As an indirect consequence, ssDNA gets longer and generates longer Rad51 filaments, which leads to higher stability after invasion. This increases the probability of crossover formation.

Rad54 may serve as an anti-recombination factor

DNA motors that prevent extensive recombination between donor and recipient molecules are characterized as anti-recombinase enzymes. This includes Sgs1/Bloom helicase (BLM), Mph1 (FANCM) and the helicase Srs2 in *S. cerevisiae* (35,93,94). Deleting these genes leads to elevated CO outcomes between donor and recipient DNA. Rad54 has been proposed to promote non-crossover outcomes as part of the synthesis dependent strand annealing pathway (SDSA) pathway (95) through its branch migration activity. A two-step mechanism has been proposed for Rad54 function at D-loops, with translocation aiding in both D-loop formation and disruption. This model suggests that second-end capture within the D-loop may be disfavored by a rate-based mechanism, reducing the probability of double Holliday junction (dHJ) formation required for CO outcomes. We offer an alternate single-step model where Rad54 may create a topological distortion of defined length in the DNA, which catalyzes the strand invasion process, maintaining under-wound DNA while Rad51 facilitates invasion (Figure 7A, B). The topological distortion would be terminated at the interface between underwound DNA and B-form DNA outside the influence of Rad54 activity. This return to B-form DNA would make termination of invasion more likely.

It is unclear how this model would affect second end capture or increase CO outcomes. However, reducing the underwound DNA, like that observed in the latch mutants, would require longer Rad51 filaments for stable invasion. While this may seem counterintuitive, longer Rad51 filaments are more likely to pair spontaneously due to favorable binding energy from higher local concentrations of Rad51, making them less dependent on Rad54 to catalyze stable invasion and more likely to overcome energy barriers associated with invading B-form DNA versus underwound DNA. Longer filaments will develop over longer periods of time and will be more resistant to disruption after formation, which could allow more efficient capture of the DNA second end within the D-loop. This would lead to increased dHJ formation and an increased probability of CO formation. Despite these possibilities, we cannot specifically conclude the biological mechanism by which the reduction in the function of Rad54 leads to an increase in CO outcomes. Possibilities include changes in Rad54 activity that alter the rate of nuclease activity at HR intermediates or increases in dHJ formation.

We observed that the deletion of *RDH54* results in further increased CO outcomes. This could occur directly by allowing increased strand invasion tracts (14) or indirectly through deregulation of Rad51 pools within the cell, as altered levels of Rad51 could increase invasion length (41,42,46,64). Each of these could cause longer strand invasion tracts, which would be more stable and prone to dHJ formation, increasing the probability of CO outcomes. While we cannot distinguish this

result as an on or off-pathway effect of Rdh54, our data suggests that latch mutations that cause a decrease in the rate of Rad54 translocation can still suppress *RAD51* overexpression phenotypes. This likely means that their defects are on-pathway and not due to changes in the available amounts of Rad51. The Rad54 latch mutants can still translocate on DNA in the presence of Rad51, which is why they can suppress this phenotype and are likely capable of removing Rad51 from dsDNA. Interestingly, the rate of Rad54 translocation is not important in suppressing this phenotype. This suggests that the translocation rate may be more important for the on-pathway activity of Rad54 during HR and less important for off-pathway activity.

Controlling the length of nascent D-loops is likely an essential feature of limiting genetic exchange

In *S. cerevisiae*, Rad54 is critical in developing proper Rad51 strand invasion intermediates. This co-dependence is less evident in higher eukaryotes, and additional factors may regulate the productive versus abortive invasion in higher eukaryotes. Factors that regulate early strand invasion intermediates include RAD51AP1 (96) and HOP2/MND1 (97,98). These factors will likely regulate D-loop intermediates through distinct mechanisms. RAD51 in higher eukaryotes may also be more stable during initial strand invasion and more readily prevent abortive invasion events. Despite this, the amino acid substitution characterized here was identified in human cancer cases and is universally conserved. This suggests that Rad54 substitutions that increase abortive invasion may also contribute to genomic rearrangements in human cancers in pathways that utilize Rad54 to mediate repair.

Data availability

All data is available upon request.

Supplementary data

Supplementary Data are available at NAR Online.

Acknowledgements

We would also like to acknowledge David Moraga, Eric Alani and Marcus Smolka for their critical manuscript reading. We would also like to thank members of the Cornell R3 group and the members of the Crickard laboratory for their helpful input during the project development.

Author contributions: K.S. performed the initial screen, genetically characterized Rad54 mutants and M.V.W. purified proteins, performed experiments, analyzed data, and helped write the manuscript. J.H. performed experiments and analyzed data. B.F. helped with the writing and editing of the manuscript. J.S. provided cloning support and critical strains. JBC performed experiments, analyzed data, provided reagents, and wrote the manuscript with input from K.S., M.V.W. and J.H. This work was supported by NIGMS R35142457 to J.B.C. and Cornell Startup funds to J.B.C.

Funding

National Institute of General Medical Sciences [NIGMS R35142457]. Funding for open access charge: NIGMS [R35142457 to the Crickard lab].

Conflict of interest statement

None declared.

References

1. Jasin,M. and Rothstein,R. (2013) Repair of strand breaks by homologous recombination. *Cold Spring Harb. Perspect. Biol.*, **5**, a012740.
2. Kowalczykowski,S.C. (2015) An overview of the molecular mechanisms of recombinational DNA repair. *Cold Spring Harb. Perspect. Biol.*, **7**, a016410.
3. Symington,L.S. and Gautier,J. (2011) Double-strand break end resection and repair pathway choice. *Annu. Rev. Genet.*, **45**, 247–271.
4. Symington,L.S., Rothstein,R. and Lisby,M. (2014) Mechanisms and regulation of mitotic recombination in Saccharomyces cerevisiae. *Genetics*, **198**, 795–835.
5. Cejka,P. and Symington,L.S. (2021) DNA end resection: mechanism and control. *Annu. Rev. Genet.*, **55**, 285–307.
6. Symington,L.S. (2014) End resection at double-strand breaks: mechanism and regulation. *Cold Spring Harb. Perspect. Biol.*, **6**, a016436.
7. Haber,J.E. (2018) DNA repair: the search for homology. *Bioessays*, **40**, e1700229.
8. Crickard,J.B., Moevus,C.J., Kwon,Y., Sung,P. and Greene,E.C. (2020) Rad54 Drives ATP hydrolysis-dependent DNA sequence alignment during homologous recombination. *Cell*, **181**, 1380–1394.
9. Qi,Z., Redding,S., Lee,J.Y., Gibb,B., Kwon,Y., Niu,H., Gaines,W.A., Sung,P. and Greene,E.C. (2015) DNA sequence alignment by microhomology sampling during homologous recombination. *Cell*, **160**, 856–869.
10. Forget,A.L. and Kowalczykowski,S.C. (2012) Single-molecule imaging of DNA pairing by RecA reveals a three-dimensional homology search. *Nature*, **482**, 423–427.
11. Renkawitz,J., Lademann,C.A. and Jentsch,S. (2014) Mechanisms and principles of homology search during recombination. *Nat. Rev. Mol. Cell Biol.*, **15**, 369–383.
12. Piazza,A. and Heyer,W.D. (2019) Moving forward one step back at a time: reversibility during homologous recombination. *Curr. Genet.*, **65**, 1333–1340.
13. Piazza,A., Shah,S.S., Wright,W.D., Gore,S.K., Koszul,R. and Heyer,W.D. (2019) Dynamic processing of displacement loops during recombinational DNA repair. *Mol. Cell*, **73**, 1255–1266.
14. Shah,S.S., Hartono,S., Piazza,A., Som,V., Wright,W., Chédin,F. and Heyer,W.D. (2020) Rdh54/Tid1 inhibits Rad51-Rad54-mediated D-loop formation and limits D-loop length. *eLife*, **9**, e59112.
15. Van Komen,S., Petukhova,G., Sigurdsson,S., Stratton,S. and Sung,P. (2000) Superhelicity-driven homologous DNA pairing by yeast recombination factors Rad51 and Rad54. *Mol. Cell*, **6**, 563–572.
16. Dumont,A., Mendiboure,N., Savocco,J., Anani,L., Moreau,P., Thierry,A., Modolo,L., Jost,D. and Piazza,A. (2023) Mechanism of homology search expansion during recombinational DNA break repair. bioRxiv doi: https://doi.org/10.1101/2023.12.01.569403, 01 December 2023, preprint: not peer reviewed.
17. Miné-Hattab,J. and Rothstein,R. (2012) Increased chromosome mobility facilitates homology search during recombination. *Nat. Cell Biol.*, **14**, 510–517.
18. Piazza,A., Bordelet,H., Dumont,A., Thierry,A., Savocco,J., Girard,F. and Koszul,R. (2021) Cohesin regulates homology search during recombinational DNA repair. *Nat. Cell Biol.*, **23**, 1176–1186.

19. Zagelbaum,J., Schooley,A., Zhao,J., Schrank,B.R., Callen,E., Zha,S., Gottesman,M.E., Nussenzweig,A., Rabadan,R., Dekker,J., *et al.* (2023) Multiscale reorganization of the genome following DNA damage facilitates chromosome translocations via nuclear actin polymerization. *Nat. Struct. Mol. Biol.*, **30**, 99–106.
20. Schrank,B.R., Aparicio,T., Li,Y., Chang,W., Chait,B.T., Gundersen,G.G., Gottesman,M.E. and Gautier,J. (2018) Nuclear ARP2/3 drives DNA break clustering for homology-directed repair. *Nature*, **559**, 61–66.
21. Dion,V., Kalck,V., Horigome,C., Towbin,B.D. and Gasser,S.M. (2012) Increased mobility of double-strand breaks requires Mec1, Rad9 and the homologous recombination machinery. *Nat. Cell Biol.*, **14**, 502–509.
22. Renkawitz,J., Lademann,C.A., Kalocsay,M. and Jentsch,S. (2013) Monitoring homology search during DNA double-strand break repair in vivo. *Mol. Cell*, **50**, 261–272.
23. Guo,X., Hum,Y.F., Lehner,K. and Jinks-Robertson,S. (2017) Regulation of hetDNA length during mitotic double-strand break repair in yeast. *Mol. Cell*, **67**, 539–549.
24. Ceballos,S.J. and Heyer,W.-D. (2011) Functions of the Snf2/Swi2 family Rad54 motor protein in homologous recombination. *Biochim. Biophys. Acta (BBA) - Gene Regul. Mech.*, **1809**, 509–523.
25. Crickard,J.B. (2021) Discrete roles for Rad54 and Rdh54 during homologous recombination. *Curr. Opin. Genet. Dev.*, **71**, 48–54.
26. Crickard,J.B. and Greene,E.C. (2019) Helicase mechanisms during homologous recombination in saccharomyces cerevisiae. *Annu. Rev. Biophys.*, **48**, 255–273.
27. Keymakh,M., Dau,J., Hu,J., Ferlez,B., Lisby,M. and Crickard,J.B. (2022) Rdh54 stabilizes Rad51 at displacement loop intermediates to regulate genetic exchange between chromosomes. *PLoS Genet.*, **18**, e1010412.
28. Antony,E., Tomko,E.J., Xiao,Q., Krejci,L., Lohman,T.M. and Ellenberger,T. (2009) Srs2 Disassembles Rad51 Filaments by a protein-protein interaction triggering ATP turnover and dissociation of Rad51 from DNA. *Mol. Cell*, **35**, 105–115.
29. Qiu,Y., Antony,E., Doganay,S., Koh,H.R., Lohman,T.M. and Myong,S. (2013) Srs2 prevents Rad51 filament formation by repetitive motion on DNA. *Nat. Commun.*, **4**, 2281.
30. Kaniecki,K., De Tullio,L., Gibb,B., Kwon,Y., Sung,P. and Greene,E.C. (2017) Dissociation of Rad51 presynaptic complexes and heteroduplex DNA joints by tandem assemblies of Srs2. *Cell Rep.*, **21**, 3166–3177.
31. Meir,A. and Greene,E.C. (2021) Srs2 and Pif1 as model systems for understanding Sf1a and Sf1b helicase structure and function. *Genes*, **12**, 1319.
32. Liu,S., Miné-Hattab,J., Villemeur,M., Guerois,R., Pinholt,H.D., Mirny,L.A. and Taddei,A. (2023) In vivo tracking of functionally tagged Rad51 unveils a robust strategy of homology search. *Nat. Struct. Mol. Biol.*, **30**, 1582–1591.
33. Jaskelioff,M., Van Komen,S., Krebs,J.E., Sung,P. and Peterson,C.L. (2003) Rad54p is a chromatin remodeling enzyme required for heteroduplex DNA joint formation with chromatin. *J. Biol. Chem.*, **278**, 9212–9218.
34. Sugawara,N., Wang,X. and Haber,J.E. (2003) In vivo roles of Rad52, Rad54, and Rad55 proteins in Rad51-mediated recombination. *Mol. Cell*, **12**, 209–219.
35. Ira,G., Malkova,A., Liberi,G., Foiani,M. and Haber,J.E. (2003) Srs2 and Sgs1-Top3 suppress crossovers during double-strand break repair in yeast. *Cell*, **115**, 401–411.
36. Alexeev,A., Mazin,A. and Kowalczykowski,S.C. (2003) Rad54 protein possesses chromatin-remodeling activity stimulated by the Rad51–ssDNA nucleoprotein filament. *Nat. Struct. Mol. Biol.*, **10**, 182–186.
37. Wolner,B. and Peterson,C.L. (2005) ATP-dependent and ATP-independent roles for the Rad54 chromatin remodeling enzyme during recombinational repair of a DNA double strand break*. *J. Biol. Chem.*, **280**, 10855–10860.
38. Petukhova,G., Stratton,S. and Sung,P. (1998) Catalysis of homologous DNA pairing by yeast Rad51 and Rad54 proteins. *Nature*, **393**, 91–94.
39. Petukhova,G., Van Komen,S., Vergano,S., Klein,H. and Sung,P. (1999) Yeast Rad54 promotes Rad51-dependent homologous DNA pairing via ATP hydrolysis-driven change in DNA double helix conformation. *J. Biol. Chem.*, **274**, 29453–29462.
40. Wright,W.D. and Heyer,W.-D. (2014) Rad54 Functions as a heteroduplex DNA pump modulated by its DNA substrates and Rad51 during D loop formation. *Mol. Cell*, **53**, 420–432.
41. Mason,J.M., Dusad,K., Wright,W.D., Grubb,J., Budke,B., Heyer,W.-D., Connell,P.P., Weichselbaum,R.R. and Bishop,D.K. (2015) RAD54 family translocases counter genotoxic effects of RAD51 in human tumor cells. *Nucleic Acids Res.*, **43**, 3180–3196.
42. Shah,P.P., Zheng,X., Epshtein,A., Carey,J.N., Bishop,D.K. and Klein,H.L. (2010) Swi2/Snf2-related translocases prevent accumulation of toxic Rad51 complexes during mitotic growth. *Mol. Cell*, **39**, 862–872.
43. Mazin,A.V., Bornarth,C.J., Solinger,J.A., Heyer,W.D. and Kowalczykowski,S.C. (2000) Rad54 protein is targeted to pairing loci by the Rad51 nucleoprotein filament. *Mol. Cell*, **6**, 583–592.
44. Wolner,B., van Komen,S., Sung,P. and Peterson,C.L. (2003) Recruitment of the recombinational repair machinery to a DNA double-strand break in yeast. *Mol. Cell*, **12**, 221–232.
45. Schmuckli-Maurer,J., Rolfsmeier,M., Nguyen,H. and Heyer,W.D. (2003) Genome instability in rad54 mutants of Saccharomyces cerevisiae. *Nucleic Acids Res.*, **31**, 1013–1023.
46. Kim,P.M., Paffett,K.S., Solinger,J.A., Heyer,W.D. and Nickoloff,J.A. (2002) Spontaneous and double-strand break-induced recombination, and gene conversion tract lengths, are differentially affected by overexpression of wild-type or ATPase-defective yeast Rad54. *Nucleic Acids Res.*, **30**, 2727–2735.
47. Goyal,N., Rossi,M.J., Mazina,O.M., Chi,Y., Moritz,R.L., Clurman,B.E. and Mazin,A.V. (2018) RAD54 N-terminal domain is a DNA sensor that couples ATP hydrolysis with branch migration of Holliday junctions. *Nat. Commun.*, **9**, 34.
48. Petukhova,G., Van Komen,S., Vergano,S., Klein,H. and Sung,P. (1999) Yeast Rad54 promotes Rad51-dependent homologous DNA pairing via ATP hydrolysis-driven change in DNA double helix conformation. *J. Biol. Chem.*, **274**, 29453–29462.
49. Morrical,S.W. (2015) DNA-pairing and annealing processes in homologous recombination and homology-directed repair. *Cold Spring Harb. Perspect. Biol.*, **7**, a016444.
50. Szostak,J.W., Orr-Weaver,T.L., Rothstein,R.J. and Stahl,F.W. (1983) The double-strand-break repair model for recombination. *Cell*, **33**, 25–35.
51. Bugreev,D.V., Hanaoka,F. and Mazin,A.V. (2007) Rad54 dissociates homologous recombination intermediates by branch migration. *Nat. Struct. Mol. Biol.*, **14**, 746–753.
52. Bugreev,D.V., Mazina,O.M. and Mazin,A.V. (2006) Rad54 protein promotes branch migration of Holliday junctions. *Nature*, **442**, 590–593.
53. Mills,K.D., Ferguson,D.O., Essers,J., Eckersdorff,M., Kanaar,R. and Alt,F.W. (2004) Rad54 and DNA Ligase IV cooperate to maintain mammalian chromatid stability. *Genes Dev.*, **18**, 1283–1292.
54. Dronkert,M.L., Beverloo,H.B., Johnson,R.D., Hoeijmakers,J.H., Jasin,M. and Kanaar,R. (2000) Mouse RAD54 affects DNA double-strand break repair and sister chromatid exchange. *Mol. Cell. Biol.*, **20**, 3147–3156.
55. Collins,B.E., Ye,L.F., Duzdevich,D. and Greene,E.C. (2014). In: Waters,J.C. and Wittman,T. (eds.) *Methods in Cell Biology*. Academic Press, Vol. **123**, pp. 217–234.
56. Crickard,J.B. (2023) Single molecule imaging of DNA-protein interactions using DNA curtains. *Methods Mol. Biol.*, **2599**, 127–139.
57. UniProt Consortium (2022) UniProt: the Universal Protein knowledgebase in 2023. *Nucleic Acids Res.*, **51**, D523–D531.

58. Waterhouse,A.M., Procter,J.B., Martin,D.M.A., Clamp,M. and Barton,G.J. (2009) Jalview Version 2—a multiple sequence alignment editor and analysis workbench. *Bioinformatics*, **25**, 1189–1191.
59. Edgar,R.C. (2004) MUSCLE: multiple sequence alignment with high accuracy and high throughput. *Nucleic Acids Res.*, **32**, 1792–1797.
60. Altschul,S.F., Madden,T.L., Schäffer,A.A., Zhang,J., Zhang,Z., Miller,W. and Lipman,D.J. (1997) Gapped BLAST and PSI-BLAST: a new generation of protein database search programs. *Nucleic Acids Res.*, **25**, 3389–3402.
61. Tate,J.G., Bamford,S., Jubb,H.C., Sondka,Z., Beare,D.M., Bindal,N., Boutselakis,H., Cole,C.G., Creatore,C., Dawson,E., *et al.* (2018) COSMIC: the catalogue of somatic mutations In cancer. *Nucleic Acids Res.*, **47**, D941–D947.
62. Kanaar,R., Troelstra,C., Swagemakers,S.M.A., Essers,J., Smit,B., Franssen,J.-H., Pastink,A., Bezzubova,O.Y., Buerstedde,J.-M., Clever,B., *et al.* (1996) Human and mouse homologs of the SaccharomycesRAD54 DNA repair gene: evidence for functional conservation. *Curr. Biol.*, **6**, 828–838.
63. Thomä,N.H., Czyzewski,B.K., Alexeev,A.A., Mazin,A.V., Kowalczykowski,S.C. and Pavletich,N.P. (2005) Structure of the SWI2/SNF2 chromatin-remodeling domain of eukaryotic Rad54. *Nat. Struct. Mol. Biol.*, **12**, 350–356.
64. Klein,H.L. (2008) The consequences of Rad51 overexpression for normal and tumor cells. *DNA Repair (Amst.)*, **7**, 686–693.
65. Hu,J., Ferlez,B., Dau,J. and Crickard,J.B. (2023) Rad53 regulates the lifetime of Rdh54 at homologous recombination intermediates. *Nucleic Acids Res.*, **51**, 11688–11705.
66. Onaka,A.T., Toyofuku,N., Inoue,T., Okita,A.K., Sagawa,M., Su,J., Shitanda,T., Matsuyama,R., Zafar,F., Takahashi,T.S., *et al.* (2016) Rad51 and Rad54 promote noncrossover recombination between centromere repeats on the same chromatid to prevent isochromosome formation. *Nucleic Acids Res.*, **44**, 10744–10757.
67. Mazin,A.V., Mazina,O.M., Bugreev,D.V. and Rossi,M.J. (2010) Rad54, the motor of homologous recombination. *DNA Repair (Amst.)*, **9**, 286–302.
68. Ho,C.K., Mazón,G., Lam,A.F. and Symington,L.S. (2010) Mus81 and Yen1 promote reciprocal exchange during mitotic recombination to maintain genome integrity in budding yeast. *Mol. Cell*, **40**, 988–1000.
69. Klein,H.L., Bačinskaja,G., Che,J., Cheblal,A., Elango,R., Epshtein,A., Fitzgerald,D.M., Gómez-González,B., Khan,S.R., Kumar,S., *et al.* (2019) Guidelines for DNA recombination and repair studies: cellular assays of DNA repair pathways. *Microb. Cell (Graz, Austria)*, **6**, 1–64.
70. Klein,H.L. (2008) The consequences of Rad51 overexpression for normal and tumor cells. *DNA Repair (Amst.)*, **7**, 686–693.
71. Reitz,D., Chan,Y.-L. and Bishop,D.K. (2021) How strand exchange protein function benefits from ATP hydrolysis. *Curr. Opin. Genet. Dev.*, **71**, 120–128.
72. Shinohara,M., Shita-Yamaguchi,E., Buerstedde,J.M., Shinagawa,H., Ogawa,H. and Shinohara,A. (1997) Characterization of the roles of the Saccharomyces cerevisiae RAD54 gene and a homologue of RAD54, RDH54/TID1, in mitosis and meiosis. *Genetics*, **147**, 1545–1556.
73. Yamaya,K., Wang,B., Memar,N., Odiba,A.S., Woglar,A., Gartner,A. and Villeneuve,A.M. (2023) Disparate roles for C. elegans DNA translocase paralogs RAD-54.L and RAD-54.B in meiotic prophase germ cells. *Nucleic Acids Res.*, **51**, 9183–9202.
74. Klein,H.L. (1997) RDH54, a RAD54 homologue in Saccharomyces cerevisiae, is required for mitotic diploid-specific recombination and repair and for meiosis. *Genetics*, **147**, 1533–1543.
75. Dürr,H., Körner,C., Müller,M., Hickmann,V. and Hopfner,K.-P. (2005) X-ray structures of the sulfolobus solfataricus SWI2/SNF2 ATPase core and its complex with DNA. *Cell*, **121**, 363–373.
76. Lewis,R., Dürr,H., Hopfner,K.P. and Michaelis,J. (2008) Conformational changes of a Swi2/Snf2 ATPase during its mechano-chemical cycle. *Nucleic Acids Res.*, **36**, 1881–1890.
77. Liu,S., Miné-Hattab,J., Villemeur,M., Guerois,R., Pinholt,H.D., Mirny,L.A. and Taddei,A. (2023) In vivo tracking of functionally tagged Rad51 unveils a robust strategy of homology search. *Nat. Struct. Mol. Biol.*, **30**, 1582–1591.
78. Tavares,E.M., Wright,W.D., Heyer,W.D., Le Cam,E. and Dupaigne,P. (2019) In vitro role of Rad54 in Rad51-ssDNA filament-dependent homology search and synaptic complexes formation. *Nat. Commun.*, **10**, 4058.
79. De Vlaminck,I., van Loenhout,M.T.J., Zweifel,L., de Blanken,J., Hooning,K., Hage,S., Kerssemakers,J. and Dekker,C. (2012) Mechanism of homology recognition in DNA recombination from dual-molecule experiments. *Mol. Cell*, **46**, 616–624.
80. van der Heijden,T., Modesti,M., Hage,S., Kanaar,R., Wyman,C. and Dekker,C. (2008) Homologous recombination in real time: DNA strand exchange by RecA. *Mol. Cell*, **30**, 530–538.
81. Ristic,D., Wyman,C., Paulusma,C. and Kanaar,R. (2001) The architecture of the human Rad54–DNA complex provides evidence for protein translocation along DNA. *Proc. Natl. Acad. Sci. U.S.A.*, **98**, 8454–8460.
82. Yang,H., Zhou,C., Dhar,A. and Pavletich,N.P. (2020) Mechanism of strand exchange from RecA-DNA synaptic and D-loop structures. *Nature*, **586**, 801–806.
83. Yang,H. and Pavletich,N.P. (2021) Insights into homology search from cryo-EM structures of RecA-DNA recombination intermediates. *Curr. Opin. Genet. Dev.*, **71**, 188–194.
84. Xu,J., Zhao,L., Xu,Y., Zhao,W., Sung,P. and Wang,H.-W. (2017) Cryo-EM structures of human RAD51 recombinase filaments during catalysis of DNA-strand exchange. *Nat. Struct. Mol. Biol.*, **24**, 40–46.
85. Kimble,M.T., Johnson,M.J., Nester,M.R. and Symington,L.S. (2023) Long-range DNA end resection supports homologous recombination by checkpoint activation rather than extensive homology generation. *eLife*, **12**, e84322.
86. Gnügge,R. and Symington,L.S. (2021) DNA end resection during homologous recombination. *Curr. Opin. Genet. Dev.*, **71**, 99–105.
87. Reitz,D., Djeghmoum,Y., Watson,R.A., Rajput,P., Argueso,J.L., Heyer,W.D. and Piazza,A. (2023) Delineation of two multi-invasion-induced rearrangement pathways that differently affect genome stability. *Genes Dev.*, **37**, 621–639.
88. Piazza,A., Wright,W.D. and Heyer,W.D. (2017) Multi-invasions are recombination byproducts that induce chromosomal rearrangements. *Cell*, **170**, 760–773.
89. Hasty,P. and Montagna,C. (2014) Chromosomal rearrangements in cancer: detection and potential causal mechanisms. *Mol Cell Oncol*, **1**, e29904.
90. León-Ortiz,A.M., Panier,S., Sarek,G., Vannier,J.-B., Patel,H., Campbell,P.J. and Boulton,S.J. (2018) A distinct class of genome rearrangements driven by heterologous recombination. *Mol. Cell*, **69**, 292–305.
91. Li,Y., Roberts,N.D., Wala,J.A., Shapira,O., Schumacher,S.E., Kumar,K., Khurana,E., Waszak,S., Korbel,J.O., Haber,J.E., *et al.* (2020) Patterns of somatic structural variation in human cancer genomes. *Nature*, **578**, 112–121.
92. Erdmann-Pham,D.D., Batra,S.S., Turkalo,T.K., Durbin,J., Blanchette,M., Yeh,I., Shain,H., Bastian,B.C., Song,Y.S., Rokhsar,D.S., *et al.* (2023) Tracing cancer evolution and heterogeneity using hi-C. *Nat. Commun.*, **14**, 7111.
93. Bugreev,D.V., Yu,X., Egelman,E.H. and Mazin,A.V. (2007) Novel pro- and anti-recombination activities of the Bloom's syndrome helicase. *Genes Dev.*, **21**, 3085–3094.
94. Prakash,R., Satory,D., Dray,E., Papusha,A., Scheller,J., Kramer,W., Krejci,L., Klein,H., Haber,J.E., Sung,P., *et al.* (2009) Yeast Mph1 helicase dissociates Rad51-made D-loops: implications for crossover control in mitotic recombination. *Genes Dev.*, **23**, 67–79.

95. Wright,W.D., Shah,S.S. and Heyer,W.D. (2018) Homologous recombination and the repair of DNA double-strand breaks. *J. Biol. Chem.*, **293**, 10524–10535.
96. Dray,E., Dunlop,M.H., Kauppi,L., San Filippo,J., Wiese,C., Tsai,M.S., Begovic,S., Schild,D., Jasin,M., Keeney,S., *et al.* (2011) Molecular basis for enhancement of the meiotic DMC1 recombinase by RAD51 associated protein 1 (RAD51AP1). *Proc. Natl. Acad. Sci. U.S.A.*, **108**, 3560–3565.
97. Chi,P., San Filippo,J., Sehorn,M.G., Petukhova,G.V. and Sung,P. (2007) Bipartite stimulatory action of the Hop2-Mnd1 complex on the Rad51 recombinase. *Genes Dev.*, **21**, 1747–1757.
98. Chan,Y.L., Zhang,A., Weissman,B.P. and Bishop,D.K. (2019) RPA resolves conflicting activities of accessory proteins during reconstitution of Dmc1-mediated meiotic recombination. *Nucleic Acids Res.*, **47**, 747–761.

Received: January 29, 2024. **Revised:** May 16, 2024. **Editorial Decision:** May 17, 2024. **Accepted:** May 21, 2024